Fuel 366 (2024) 131269

Contents lists available at ScienceDirect

Fuel

journal homepage: www.elsevier.com/locate/fuel

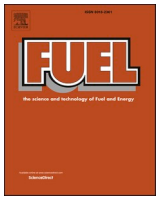

Full Length Article

Kerosene production from power-based syngas – A technical comparison of the Fischer-Tropsch and methanol pathway

Stefan Bube *, Nils Bullerdiek, Steffen Voß, Martin Kaltschmitt

Hamburg University of Technology (TUHH), Institute of Environmental Technology and Energy Economics (IUE), Eißendorfer Straße 40, 21073 Hamburg, Germany

ARTICLE INFO

Keywords:
Power-to-Liquid (PtL)
Sustainable Aviation Fuel (SAF)
Fischer-Tropsch (FT) Synthesis
Power-to-Methanol (PtM)
Methanol-to-Kerosene
E-fuel

ABSTRACT

To achieve long-term greenhouse gas (GHG) neutrality within the aviation sector, substituting fossil aviation fuels with Sustainable Aviation Fuels (SAF) derived from renewable energy sources is essential. Among the synthetic SAF options produced through Power-to-Liquid (PtL) processes, the Fischer-Tropsch (FT) and methanol pathway are of significant interest. However, to assess and compare these pathways, detailed technical process analyses are required to provide a sound basis for economic and environmental assessments. Thus, this research paper investigates and compares both SAF production pathways starting from power-derived syngas within an in-depth technical analysis, providing novel insights into overall process characteristics and efficiencies. Carbon and energy flows are derived from steady-state flowsheet simulations. A variation of technical parameters (FT pathway: FT chain growth probability and hydrocracking behavior, Methanol pathway: Dehydration olefin-selectivity and oligomerization product distribution) is carried out to assess impacts on carbon and energy efficiency, indicating uncertainties and parameter ranges for optimized kerosene production. The results show a very high carbon efficiency of the FT pathway (98 to 99%) regarding the total liquid products, while the carbon efficiency regarding kerosene lies between 60 and 77%. For the methanol pathway, a higher kerosene carbon efficiency can be achieved (60 to 90%); however, the total product efficiency (74 to 92%) is notably lower. The energy efficiencies of both pathways behave similarly to carbon efficiency, with the methanol pathway benefiting from thermodynamic advantages, leading to higher energy efficiency at equal carbon efficiency. Within the FT pathway, kerosene efficiency increases at high chain growth probabilities, while a high olefin-selectivity is crucial for efficient kerosene production within the methanol pathway. The analysis results provide comprehensive insights into the technical behavior of the overall processes which contributes to an improved understanding of the production pathways.

1. Introduction

The global aviation sector shows a significant disparity between the targeted and projected greenhouse gas (GHG) emissions. On the one hand, both the International Civil Aviation Organization (ICAO) as well as the International Air Transport Association (IATA) have announced the goal of reducing CO_2 emissions to net zero by 2050 [1,2]. On the other hand, demand for air transportation increases continuously worldwide, resulting in increasing aviation-related CO_2 emissions if no appropriate measures are implemented [3]. To decouple the projected growth in aviation from an increase in GHG emissions and achieve long-term GHG neutrality, fossil fuel-based aviation fuels need to be increasingly replaced by fuel options based on renewable energy sources. From today's perspective, the use of carbon-free energy carriers

Abbreviations: ASF, Anderson-Schulz-Flory; ASTM, American Society for Testing and Materials; AtJ, Alcohol-to-Jet; DAC, Direct air capture; FT, Fischer-Tropsch; GHG, Greenhouse gas; HEFA, Hydroprocessed Esters and Fatty Acids; HHV, Higher heating value; IATA, International Air Transport Association; ICAO, International Civil Aviation Organization; K, Kerosene; LTFT, Low-temperature Fischer-Tropsch; MOGD, Mobil olefins to gasoline and distillate; MtHC, Methanol-to-Hydrocarbon; MtJ, Methanol-to-Jet; MtK, Methanol-to-Kerosene; MtO, Methanol-to-Olefins; Oli, Oligomerization; PtL, Power-to-Liquid; PV, Parameter variation; RC, Reference case; RWGS, Reverse water–gas shift; SAF, Sustainable Aviation Fuel; SPA, Solid phosphoric acid; TP, Total product; TRL, Technology readiness level; W, Wax.

* Corresponding author.
E-mail address: stefan.bube@tuhh.de (S. Bube).

[1] Unlike climate-effective CO_2 emissions, aviation-related non-CO_2 effects cannot be fully mitigated by the combustion-based utilization of such fuel [4,5]. Non-CO_2-effects are effects that are not directly related to the emission of CO_2 but also contribute to global warming. Examples are e.g., contrail formation or NO_x and sulfur emissions.

https://doi.org/10.1016/j.fuel.2024.131269
Received 21 September 2023; Received in revised form 8 February 2024; Accepted 20 February 2024
Available online 1 March 2024

used in respective aircraft concepts (e.g., liquid hydrogen or battery-electric aircraft) appears to be rather challenging and, if at all, technologically only feasible in the longer term, as this requires the design of fully new aircraft and a built-up of a proper fuel infrastructure alongside with the existing aviation fuel infrastructure for kerosene-type aviation fuels [6,7].

Against this background, renewable aviation fuels should not only provide significantly lower GHG emissions, but also be technically compatible with existing aircraft fleets and fuel infrastructure used for conventional kerosene so far. Such kerosene-type fuels that can be produced based on renewable energy sources are commonly referred to as Sustainable Aviation Fuels (SAF)[1].

Different process pathways enable the utilization of various energetic (e.g., biomethane, electrical power) and material feedstock options (e.g., carbon dioxide, water) for kerosene-type fuel production. Currently, commercially used SAFs are almost exclusively produced based on vegetable oils and lipid wastes such as Hydroprocessed Esters and Fatty Acids (HEFA). In addition, with the start-up of the first production facilities, a ramp-up of conversion processes, mainly for advanced bio-kerosene production, is taking place [8]. However, due to the a priori limited potential of sustainable provided biomass and the much-discussed plate vs. tank issue, a massive expansion of these types of bio-kerosene to cover the existing as well as the emerging demand is doubtful [9]. Alternatively, fuels from renewable electricity and sustainable CO_2 (e-fuels) can be a promising fuel option characterized by a clearly greater production potential. The production of such e-fuels through so-called Power-to-Liquid (PtL) processes takes place via power-based synthesis gas (syngas) production, a synthesis step, and the subsequent downstream processing; thus, the fuels are also referred to as synthetic fuels. As of today, the main process routes discussed are the Fischer-Tropsch (FT) and the methanol pathway. While SAF from FT processes is already approved according to ASTM D7566 as drop-in aviation fuel, the approval of methanol-based SAF production is currently undergoing the respective approval process (ASTM D4054). Accordingly, there are presently no methanol-to-kerosene production plants in commercial operation. However, methanol-based aviation fuel is a frequently discussed option, offering potential advantages against other production routes [10].

1.1. Conversion pathways

Power-based SAF production starts from the feedstocks water (H_2O) and carbon dioxide (CO_2). The energy converted into the chemical energy of the fuel and the energy needed for processing is primarily provided in the form of electricity. Electrochemical water splitting (electrolysis) produces hydrogen (H_2), and CO_2 is provided via capturing processes from respective "sustainable" carbon sources. Starting from these two gases, the FT- and methanol-based conversion pathway differ in the subsequent process chain (Fig. 1).

1.1.1. Fischer-Tropsch pathway

The FT synthesis from carbon monoxide(CO)- and H_2-rich syngas is a state-of-the-art technology with its first commercial implementation in the 1930s [11,12]. However, the direct conversion of CO_2 into long-chain hydrocarbons is not yet feasible with sufficient selectivity and conversion and requires further research for future applications [12,13]. Thus, a CO_2 reduction to CO is needed to provide appropriate syngas for the subsequent kerosene production. Converting H_2 and CO into hydrocarbon chains within the FT synthesis yields synthetic crude oil (syncrude), ranging from light gases (e.g., methane) to long-chain hydrocarbons (waxes). Therefore, producing specification-compliant aviation fuel requires further downstream refining by hydrotreatment and fractionation. Thereby, unsaturated hydrocarbons are saturated (hydrogenation), and waxes can be converted into fuel components by chain breaking (hydrocracking). If the cold flow properties required by the ASTM D7566 specification are not reached, additional hydroisomerization can be applied for branching the linear molecules.

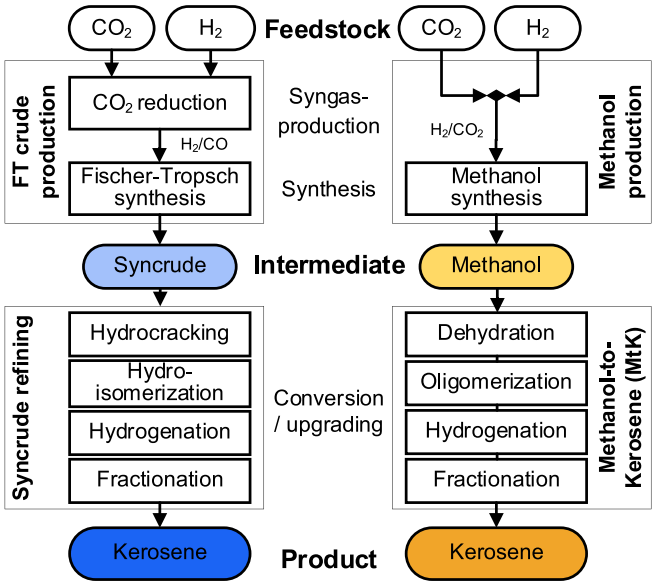

Fig. 1. Fischer-Tropsch- and methanol-based kerosene production pathways.

1.1.2. Methanol pathway

The methanol pathway can be divided into the actual methanol synthesis, allowing highly selective methanol production, and the subsequent conversion of methanol into a hydrocarbon fuel mixture rich in kerosene components (Methanol-to-Kerosene (MtK), also Methanol-to-Jet (MtJ)). Methanol synthesis enables the direct conversion of CO_2 and H_2 into methanol, making a previous CO_2 reduction obsolete. The CO_2-based methanol synthesis yields a mixture of methanol and water subsequently separated through distillation. Processes to convert methanol into hydrocarbons were developed mainly in the 1970s and commercialized in the 1980s [14,15]. However, the focus was rather on producing products with a shorter carbon chain length, such as gasoline. Thus, no kerosene-specific concepts have been implemented to date. Like all alcohol-based conversion routes (Alcohol-to-Jet (AtJ)), the methanol to kerosene conversion includes olefin formation within a dehydration process and a subsequent oligomerization into higher olefins. Further downstream hydrogenation converts the unsaturated hydrocarbons to alkanes, which are subsequently fractionated via distillation processes to obtain the desired fuel fractions [16].

1.2. Target and scope

The above-presented background highlights the necessity of renewable aviation fuels in air transport and the potential significance of both process routes for electricity-based SAF production. However, comprehensive analyses are currently lacking a technical comparison of the FT and methanol pathway, preventing detailed economic and environmental studies. Atsonios et al. recently analyzed different production routes for e-kerosene in terms of carbon utilization and energy efficiency, with the results indicating particular advantages of the FT pathway [17]. However, the comprehensive analysis focuses on comparing several process routes based on fixed process assumptions, whereby no analysis of specific influencing variables was carried out. Further studies are therefore required to identify uncertainties and optimization potentials and to contribute toward enhanced process understanding.

Against this background, this research paper aims to assess and compare the production of synthetic kerosene from power-derived syngas via the Fischer-Tropsch and the methanol pathway within a technical analysis. Novel results arise particularly from the in-depth

investigation of the process concepts and assessing critical process parameters regarding their impacts on process efficiencies. Fig. 2 depicts the considered system boundaries within a generic supply and production chain.

The analysis focuses on the synthesis and downstream processes, considering H_2 and CO_2 as given feedstocks. A synthetic kerosene fraction represents the target product of both pathways at the end of the system boundaries considered. Thus, subsequent refining, logistics, or blending steps are not relevant for the comparative evaluation of the two production pathways and, therefore, not covered by the system boundaries of this analysis. A steady-state flowsheet simulation of the processes forms the basis of the analysis. The results of the reference cases are presented in carbon and energy flow diagrams. An extensive variation of the most critical parameters is carried out to estimate technical uncertainties and the influences of different process properties regarding carbon and energy efficiency.

2. Methodology

The technical analysis and comparison of kerosene production via the Fischer-Tropsch and the methanol pathway is based on an analysis of important technical key figures (here: carbon and energy efficiency) and the respective sensitivities. The overall assessment approach applied is shown in Fig. 3. Following this, the design and simulation of reference production concepts are used as a basis for the subsequent process analysis and evaluation. The simulation results are utilized for visualizing and evaluating the carbon and energy flows, enabling a comprehensive understanding of the processes. Within the process assessment, the influences of selected technology parameters on the key figures – and thus the resulting uncertainties and optimization possibilities – are evaluated through parameter variations. The applied steps, software tools, and methods are described below.

2.1. Process design

Process modeling and simulation are based on the design of representative and fair-comparable processes (reference concepts). The design of such processes depends on the assumed feedstock and the desired target product. Based on these cornerstones, the reference concepts are developed by integrating single reference processes. Only subprocesses with a technology readiness level (TRL) ≥ 6 are considered. This procedure ensures that the reference concepts can be commercially realized in the short-term – at least from a technical perspective. All process data – i.e., conversion rates, selectivities, and operating conditions – are based on literature and adapted to a kerosene-maximized production. Side-products in the fuel range of naphtha (gasoline) and diesel are considered valuable outputs; i.e., no "kerosene-only" concepts are considered.

2.2. Process modeling and simulation

A steady-state flowsheet simulation determines the mass and energy flows in the analyzed processes. For this purpose, the reference concepts are modeled using the commercial simulation software Aspen Plus®, allowing to determine the occurring material and energy streams based on well-approved thermodynamic calculation methods and material databases. Therefore, the considered components and the applied property methods are specified. The process flowsheet can be modeled using preconfigured or specially constructed unit operations [18]. The respective process blocks are connected with material, heat, or power streams. No internal integration of heat streams is assumed within the simulation model. Further information on the simulation program can be found in the specialist literature [19–21].

A pinch analysis using the Aspen Energy Analyzer® is carried out to address heat integration appropriately, providing information on the minimal external heating and cooling demands. Based on the simulated heat flows, the heat integration is approximated without the specific design of equipment. The minimum temperature differences of the heat transfer and the available "external" utilities are chosen within the model.

2.3. Process assessment

For the analysis of the simulation results, the derived mass and energy balances from the process modeling are used to determine technical key figures of the overall process. Therefore, two assessment figures – carbon and energy efficiency – are defined. The sensitivity of these assessment figures is analyzed based on a parameter variation.

Both key figures are related to the production of kerosene (K) as the target product as well as to the total liquid product (TP), including the naphtha (gasoline), kerosene, and diesel fraction.

2.3.1. Carbon efficiency

Carbon efficiency is a product-independent comparative figure for material efficiency due to its molar reference. Furthermore, the limited availability of sustainable carbon from biomass underlines the need for efficient carbon use as it directly impacts economic competitiveness. It indicates the selectivity of the process concerning the target product relative to the input material; i.e., this figure describes the amount of carbon bound in the target product compared to the amount of carbon contained in the feedstock (Eq. (1)). The reference to molar carbon enables a comparison independent of the actual mass of the substance used or the product obtained.

$$\eta_{C,\ Product} = \frac{\dot{C}_{Product}}{\dot{C}_{Feed}} \tag{1}$$

η_C Carbon efficiency [-].$\dot{C}$ Carbon flow [mol_C/s].

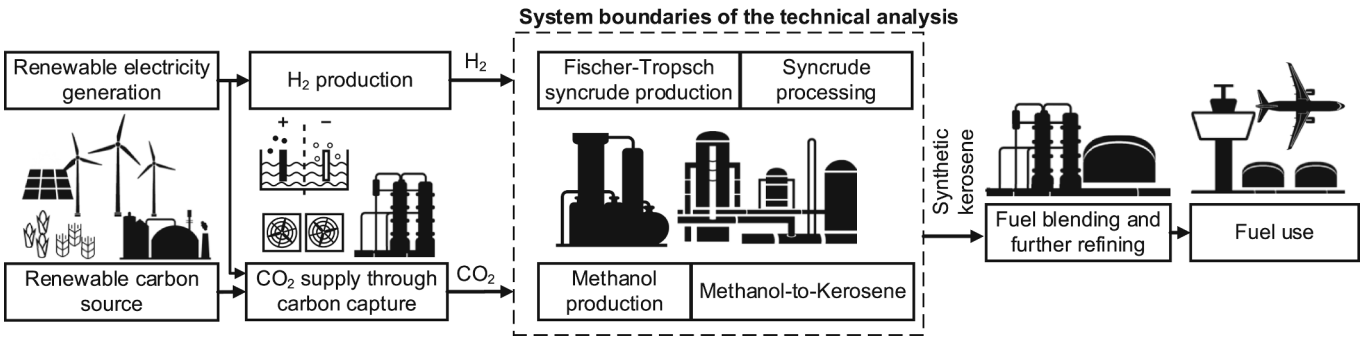

Fig. 2. System boundaries within a generic supply chain of power-based Fischer-Tropsch and methanol-based kerosene production.

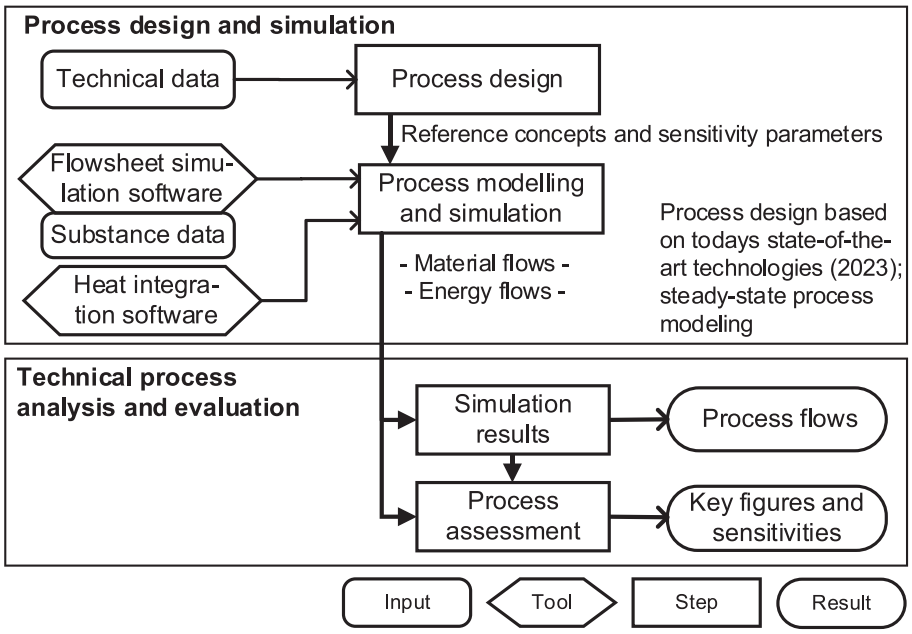

Fig. 3. Overarching assessment approach.

2.3.2. Energy efficiency

Energy efficiency is a commonly used key figure allowing to assess processes regarding their overall energy expenditure. Here, energy efficiency describes the energy content of the product compared to the energetic effort of production (i.e., chemical energy from the feedstock plus additionally needed electrical and thermal process energy) (Eq. (2)). Here, chemical energy is always related to the energy carrier's higher heating value (HHV), unless otherwise stated.

$$\eta_{e,\ \mathrm{Product}} = \frac{\dot{m}_{\mathrm{Product}}\,\mathrm{HHV}_{\mathrm{Product}}}{\dot{m}_{\mathrm{Feed}}\,\mathrm{HHV}_{\mathrm{Feed}} + P_{el} + \dot{Q}} \tag{2}$$

η_e Energy efficiency [-].$\dot{m}$ Mass flow [kg/s].HHV Higher heating value (HHV) [MJ/kg].P_{el} External electricity demand [MW].$\dot{Q}$ External heat demand [MW].

3. Reference concepts and data

This section describes the defined reference concepts. A detailed description of the technologies considered can be found in the supplementary information, section 1. According to Fig. 1, both pathways are distinguished into two process sections.

3.1. Reference concepts

3.1.1. Process inputs and output

The provision of power-based H_2 and sustainable CO_2 falls outside the system boundaries of this analysis. Thus, it is assumed that H_2 at 50 bar (i.e., a pressure level achievable with advanced low-temperature electrolyzers [22,23]) and CO_2 are available at the plant; the latter is available at atmospheric pressure with a concentration of 99 vol-% CO_2 and 1 vol-% nitrogen (N_2) [24]. Concerning the carbon chain length, the target product kerosene is defined as the C_8 to C_{16} fraction of the hydrocarbon product mixture [25,26]. Besides kerosene, a light naphtha fraction (C_5 to C_7) and a heavy diesel fraction (C_{17} to C_{20}) are considered valuable side-products. Further material outputs like fuel gas are considered to be burned for energy recovery within both pathways.

3.1.2. Fischer-Tropsch pathway

The Fischer-Tropsch pathway includes the process sections "FT syncrude production" and "Syncrude refining".

3.1.2.1. Fischer-Tropsch syncrude production. Fig. 4 shows the flowsheet of the FT syncrude production section. The process uses a low-temperature Fischer-Tropsch (LTFT) synthesis, enabling the production of a paraffinic syncrude that is well-suited for kerosene production. A CO and H_2-rich syngas is required, as CO_2 behaves inertly under most LTFT catalysts [11,12,27]. FT synthesis with direct CO_2 utilization is a promising alternative and the focus of current research. However, thus far, this has only been demonstrated on a small scale and at higher temperatures for producing olefins, aromatics, and short-chain fractions [28–31]. Thus, applying power-based syngas today requires an additional CO_2-reduction step, here considered via a reverse water–gas shift (RWGS) reaction (Eq. (3)) [12].

$$CO_2 + H_2 \rightleftharpoons CO + H_2O \,|\, \Delta H_{R(298K)} = 42\,\mathrm{kJ/mol} \tag{3}$$

First, CO_2 is compressed together with the synthesis loop recycle gas, mixed with H_2, and heated up to 950 °C to enable high conversion rates and to avoid coking at the catalyst. The RWGS reactor is assumed to operate isothermally, providing the required heat via electrical heating. The reaction product is dried by cooling and condensation before it is fed to the FT reactor. Due to the elevated RWGS operation pressure (26 bar), intermediate compression between the reactors is avoided. Eq. (4)

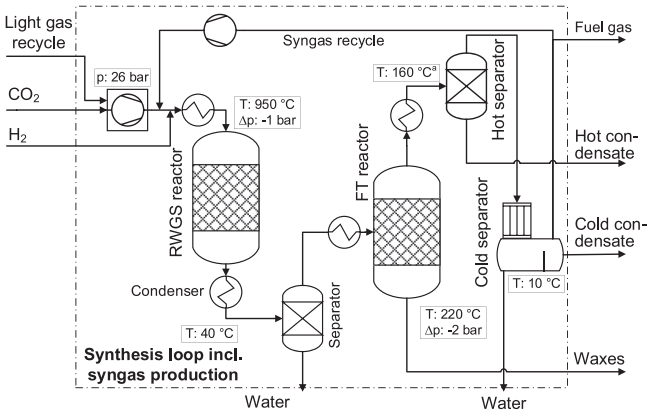

Fig. 4. Fischer-Tropsch syncrude production flowsheet ([a] temperature control prevents water condensation. Minor equipment and auxiliary currents are neglected; RWGS: Reverse water–gas shift).

shows the strongly exothermic FT reaction. The Anderson-Schulz-Flory (ASF) distribution (Eq. (5)) can describe the chain length distribution of the FT product. The chain length-dependent olefin to paraffin formation can be described with Eq. (6) [32].

$$nCO + (2n+1)H_2 \rightarrow C_nH_{2n+2} + nH_2O \,|\, \Delta H_{R(298K)} \approx n(-150 kJ/mol) \quad (4)$$

$$W_n = n(1-\alpha)^2\alpha^{n-1} \quad (5)$$

$$(O/P)_n = e^{-c\,n} \quad (6)$$

n Carbon chain length [-].W_n Weight fraction [wt-%].α Chain growth probability [-].O/P Olefin to paraffin ratio [-].*c* Adjustment parameter [-].

The FT syncrude is separated into three different liquid streams – a liquid wax fraction, a hot condensate, and a cold condensate. The wax fraction is already liquid under reaction conditions and can be directly separated from the gaseous product stream. Depending on the reactor design, the liquid wax phase separation can already occur in the reactor or downstream in a conventional gas/liquid separator. The gas phase is cooled to about 160 °C in a first separator, where an additional waxy hot condensate can be separated, but parallel water condensation is avoided. In a cold separator, the remaining gas is further cooled to about 10 °C to condense lighter hydrocarbons and water, which can be decanted as a separate liquid phase. The remaining light gases – consisting mainly of N_2 accumulations, unconverted reactants (H_2, CO), CH_4, and CO_2– are recycled and partly purged (fuel gas). Since cobalt-catalyzed LTFT only enables the conversion of CO, with CO_2 and hydrocarbons behaving inertly, internal recycling of short-chain products is not considered. However, external recycling – i.e., recycling, which includes equipment outside the FT synthesis loop, is considered with the co-reforming of light C_1 to C_4 hydrocarbons in the RWGS reactor [33].

3.1.2.2. Syncrude refining. The technologies and the configuration of the FT downstream processing depend mainly on the applied FT synthesis technology and the target products. With a prioritized production of kerosene, extensive hydrotreatment (including hydrogenation, hydrocracking, and/or hydroisomerization (see supplementary information, section 1), is required. In addition, the thermal separation process of rectification is applied to separate the different fuel fractions (fractionation).

The flowsheet of the FT syncrude refining is shown in Fig. 5. The wax fraction is mixed with hot condensate and hydrogen before the mixture is heated and fed to the hydrocracking reactor. The product consists of various saturated hydrocarbons fractionated within a downstream-located rectification column. Heavy components ($\geq C_{21}$) are fed back for further cracking, while a lighter kerosene/diesel fraction and a light gas/naphtha fraction are extracted for additional separation. Since the combination of LTFT synthesis and downstream hydrocracking – with parallel isomerization – leads to a product mixture with high proportions of singly branched hydrocarbons, separate hydroisomerization is most likely not necessary [26,34]. The cold condensate is rectified to separate light gases and naphtha from the heavier fractions. The light stream is separated in another column into naphtha and light gas, where the latter is recycled back to the synthesis section. The bottom stream from the middle (distillate) column is hydrogenated and fractionated to derive the desired kerosene fraction and diesel as a by-product.

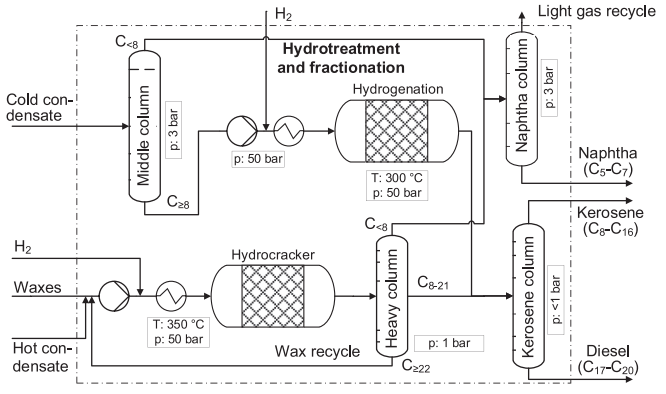

Fig. 5. FT syncrude refining flowsheet (minor equipment and auxiliary currents neglected).

3.1.3. Methanol pathway

The methanol pathway is distinguished into the process sections "Methanol production" and the subsequent "Methanol-to-Kerosene".

3.1.3.1. Methanol production. The direct synthetic conversion of CO_2 via direct methanol synthesis is already demonstrated and commercially realized on a small scale (TRL 8 to 9) [12,26]. Thus, starting from pure H_2 and CO_2, syngas is produced by mixing both substances in the required ratio. The stoichiometric number (*SN*) can quantify the intended ratio on a molar level (Eq. (7)). Within the methanol synthesis (Eq. (8)), slightly over-stoichiometric ratios of 2.05 to 2.10 are realized, positively affecting the synthesis [14,35,36].

$$SN = \frac{[H_2]-[CO_2]}{[CO]+[CO_2]} \quad (7)$$

SN stoichiometric number [-].[X] molar fraction of component X [-].

$$CO_2 + 3\,H_2 \rightleftharpoons CH_3OH + H_2O \,|\, \Delta H_{R(298\,K)} = -49.2\,kJ/mol \quad (8)$$

Fig. 6 shows the flowsheet for a direct CO_2-converting methanol synthesis. As shown, CO_2 and H_2 are fed into a multi-stage syngas compressor and mixed with light gases from the first purification column, which mainly consist of CO_2. The compressed gas stream is then mixed with recycled syngas and preheated before it is fed into the methanol reactor. The reaction product is cooled and partially condensed. Part of the unconverted syngas is purged out of the process to avoid an accumulation of inert gases or light synthesis by-products. The remaining part of the gas phase is compressed again to overcome the pressure drop of the synthesis reactor. The liquid raw methanol, a mixture of mainly methanol, water, and solved gases, is fed to the so-called topping column, where the solved gases and light by-products are separated from the mixture. The methanol–water mixture builds the bottom product and is fed to the methanol column to provide pure methanol as the main product.

3.1.3.2. Methanol-to-Kerosene process. The Methanol-to-Kerosene (MtK)

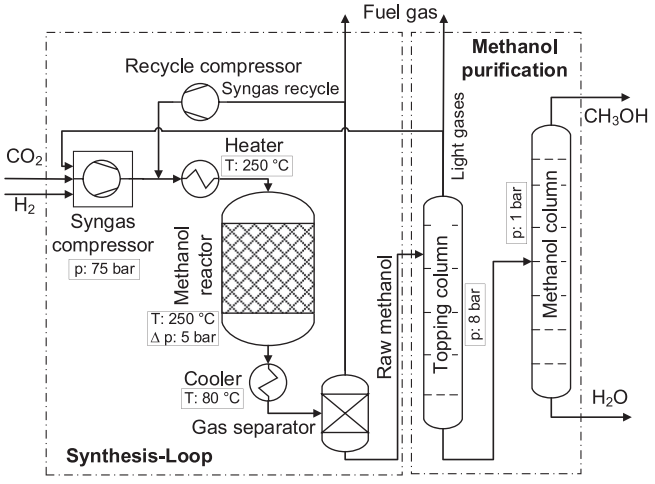

Fig. 6. Methanol production flowsheet (minor equipment and auxiliary currents neglected).

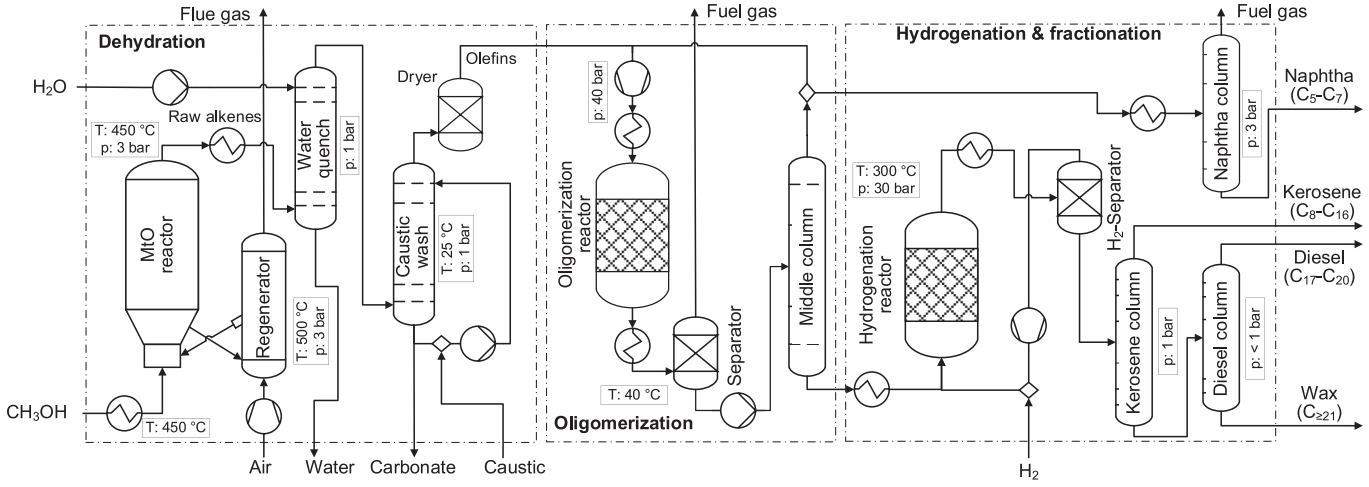

Fig. 7. Methanol-to-Kerosene flowsheet with main components (minor equipment and auxiliary currents neglected).

process, analogous to common alcohol-to-hydrocarbon processes, consists of dehydration, oligomerization, and hydrogenation (supplementary information, section 1). The decisive factor for the product formed is the combination of dehydration and oligomerization.

Fig. 7 shows the process flowsheet of the MtK process derived. The methanol is compressed and enters the MtO reactor to generate light olefins. The MtO section is designed based on the UOP/Norsk Hydro MtO process without further olefin separation [16]. The raw olefin stream is then fed in a water separation column and subsequently washed with caustic soda for CO_2 separation. After the olefin stream is further dried through a molecular sieve, it enters the oligomerization unit. The product distribution of most oligomerization processes can be approximated with a generic ASF distribution [37–39]. Considering that the starting point of the distribution – i.e., regarding the product with the shortest carbon chain length – is affected by the carbon chain length of the olefin feedstock, the adjusted ASF distribution can be described by Eq. (9).

$$W_n = (n - x - 1)(1 - \alpha)^2 \alpha^{n-x-2} \quad \text{for } n \geq x \tag{9}$$

n Carbon chain length [-].W_n Weight fraction [wt-%].α Chain growth probability [-].x Adjustment parameter [-].

The weight fraction (W_n) of the product with the chain length (n) depends on the chain growth probability (α) and the starting point adjustment variable x. Assuming a complete per-pass conversion, $x = 2$ represents an ethene-ethene, $x = 3$ an ethene-propene, and $x = 4$ a propene-propene dimer as the lightest component. For the formation of hydrocarbons in the kerosene range, operating conditions from 150 to 300 °C and 40 to 100 bar seem practical [14,15]. The oligomerization reactor product is cooled to 40 °C to separate light MtO by-products, predominantly light alkanes. To achieve a maximized kerosene output, the liquid stream is fed into a distillation column, which further separates light gases and naphtha from the higher olefins. The light fraction is mainly recycled to the oligomerization reactor, while a purge stream is extracted to avoid an accumulation of higher alkanes. Multi-stage oligomerization is also conceivable, but due to the generic modeling approach, it is not considered here. The bottom stream of the column is then hydrogenated and fractionated.

3.2. Data and assumptions

The following section outlines the most important data and assumptions of process modeling. For additional modeling data, refer to the supplementary information, section 2.

3.2.1. Fischer-Tropsch pathway

3.2.1.1. Fischer-Tropsch syncrude production. Table 1 presents the most important parameters and assumptions for modeling the FT syncrude production. The RWGS product mixture is assumed to be in a chemical equilibrium at the applied operating conditions (i.e., fast kinetics at these temperatures) [40]. The operating pressure of the FT reactor and the pressure drop of the RWGS reactor determine the outlet pressure of the syngas compression, avoiding intermediate compression. The H_2:CO ratio in the FT feed is set to 2.05. The total share of reactants (CO and H_2) is set to 70 %, with the rest resulting from accumulated inert components and unconverted RWGS products (CH_4 and CO_2). The chain growth probability (Eq. (5)) differs depending on the process technology, which is varied to evaluate the influence on the overall process. Within the reference case, chain growth probability is set to yield a maximum straight-run kerosene fraction. Some of the considered ASF distributions are exemplarily shown in Fig. 8 (left). However, the selectivities for C_1 and C_2 products deviating from the actual ASF are adjusted in the model according to [11]. High-temperature (HT)

Table 1
Key modeling parameter of the FT syncrude production (RC: Reference case, *T*: Temperature, *p*: Pressure, PV: Parameter variation).

Process	Parameter		Value	Reference
RWGS reactor	Operating conditions	T [°C]	950	[26,33,34]
		$p_{in} \mid \Delta p$ [bar]	26 | −1	[26,33]
	Equilibrium conversion	Products considered: CO, CO_2, H_2O, H_2, CH_4		[41,42]
FT reactor	Operating conditions	T [°C]	220	
		$p_{in} \mid \Delta p$ [bar]	25 | −2	[12,34,43]
	Reaction parameter	Chain growth probability (Eq. (5))[a]	RC: 0.85 PV: 0.75–0.95[b]	[11]
		Per-pass conversion [%]	65	[12]
	By-product formation	c in olefin share (Eq. (6))	0.3	[32]

[a] C_1 to C_2 selectivity adjusted according to [11], [b] see supplementary information, section 2.2.

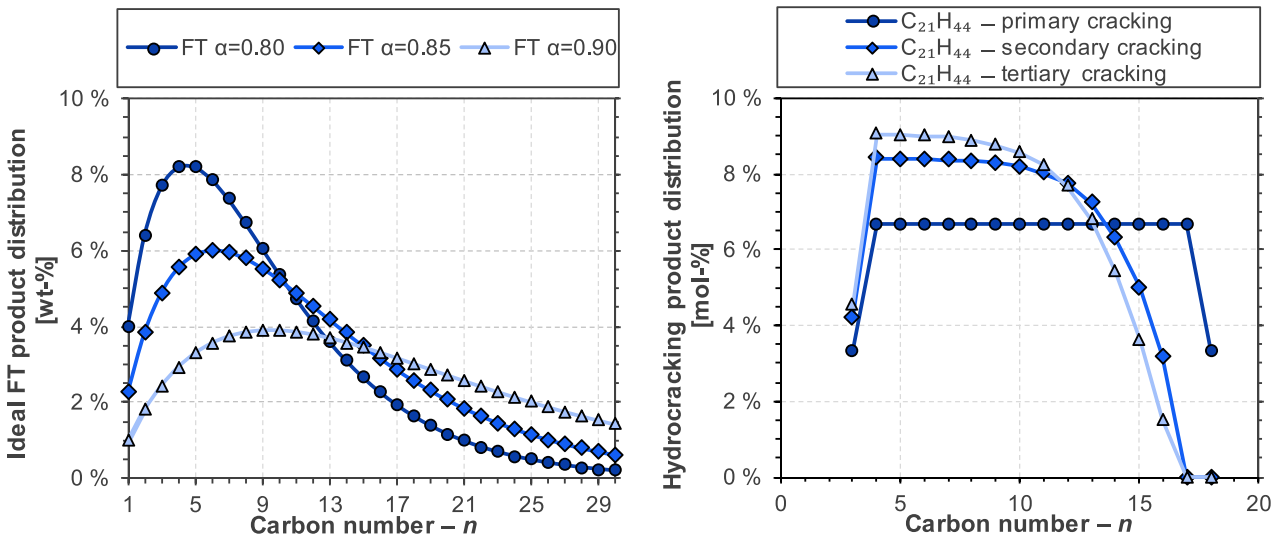

Fig. 8. Exemplary FT and hydrocracker product distributions according to model assumptions (α: Chain growth probability; FT: Fischer-Tropsch).

condensate is separated under the restriction that water condensation is avoided (temperature control). Cold condensate is separated at 10 °C to avoid recycling of higher alkanes to the RWGS reactor.

3.2.1.2. Syncrude refining. Table 2 shows data and assumptions for the syncrude refining concept.

Ideal hydrocracking is assumed [45]. The selectivities to all C_4 to C_{n-4} products derived from a C_n reactant are equal, while the selectivities to C_3 and C_{n-3} products are assumed to be only half as high. Products with a carbon chain length $< C_2$ are not formed. Since the cracking activity of hydrocarbons increases exponentially with increasing carbon chain length, the conversion is determined component-specifically between C_8 and C_{17} using an exponential function. No reaction is assumed for hydrocarbon chains smaller than C_8, while components larger than C_{17} are completely converted. In the reference case, each cracked component can undergo secondary cracking with a probability dependent on its new chain length. To evaluate the influence of different hydrocracking behaviors, the process assessment also takes into account single cracking (primary) and triple cracking (tertiary). The resulting product distributions using the example of a single component are shown in Fig. 8 (right).

3.2.2. Methanol pathway

3.2.2.1. Methanol production. Essential assumptions and data used for modeling the methanol production section are presented in Table 3. The syngas conversion is assumed to be close to equilibrium using a temperature approach [14,47]. The formation of by-products is considered proportional to the methanol formation and calculated from selectivity data according to [12]. To account for occurring syngas losses due to purge gas, the purge gas volume is adjusted to achieve a common recycle ratio of 4.5 [12,48]. The rectification columns are designed so that the effluent meets the purity requirements of internationally traded methanol. Since no significant uncertainties regarding the modeling of the methanol synthesis are evaluated, no sensitivity parameters are considered.

3.2.2.2. Methanol-to-Kerosene process. Table 4 shows the key modeling data of the Methanol-to-Kerosene process section. Since the olefin-selectivity of the MtO reaction is decisive for the assumed oligomerization and literature values differ, its influence is investigated through parameter variation. Therefore, the respective MtO reactions are adjusted by an olefin-selectivity factor (S_o). Oligomerization is modeled generically according to Eq. (9). Since MtO can yield olefins in the range

Table 2
Key modeling parameter of the syncrude refining (RC: Reference case, *T*: Temperature, *p*: Pressure, PV: Parameter variation).

Process	Parameter		Value	Reference
Hydrocracker	Operating conditions	*T* [°C] | *p* [bar]	350 | 50	[34,44,45]
	Reaction parameter	Ideal cracking with chain length depending conversion; RC: Secondary cracking; PV: Primary to tertiary cracking		Based a.o. on [26,45]
Hydrogenation	Operating conditions	*T* [°C] | *p* [bar]	300 | 40	[44,46]
	Reaction parameter	Conversion [%]	100	[44,46]

Table 3
Key modeling data of the methanol production (DME: Dimethyl ether, *T*: Temperature, *p*: Pressure).

Process	Parameter		Value	Reference
Methanol reactor	Operating conditions	*T* [°C]	250	[12]
		p_{in} | Δp [bar]	75 | −5	[12,49,50]
	Equilibrium conversion with temperature approach	$CO + 2\ H_2 \leftrightharpoons CH_3OH$	15 K	[47]
		$CO_2 + 3\ H_2 \leftrightharpoons CH_3OH + H_2O$	15 K	[47]
		$CO_2 + H_2 \leftrightharpoons CO + H_2O$	15 K	[47]
	By-product formation	Ethanol | DME | methyl format [w ppm]	89 | 145 |14	[12]
Syngas purge	Recycle gas ratio [a] [mol%], controlled by syngas purge		450	[12,48]

[a] Ratio = Recycle (mol/s)/fresh gas (mol/s).

Table 4
Key modeling data of the Methanol-to-Kerosene process (RC: Reference case, MtO: Methanol-to-Olefins, p: Pressure, PV: Parameter variation, S_O: Olefin-Selectivity, T: Temperature).

Process	Parameter		Value	Reference
MtO reactor	Operating conditions	T [°C] | p [bar]	450 | 3	[51,52]
	Reaction parameter	Olefin-selectivity (S_O) [%$_C$][a]	RC: 90; PV: 85–95	[53–57]
		Conversion [%]	100	[51,52,57]
	Reactionconversion [%]	2 $CH_3OH \rightarrow C_2H_4 + 2\ H_2O$	46.00 • S_O	according to
		3 $CH_3OH \rightarrow C_3H_6 + 3\ H_2O$	42.89 • S_O	[53,54,58–60]
		4 $CH_3OH \rightarrow C_4H_8 + 4\ H_2O$	11.11 • S_O	
		13 $CH_3OH \rightarrow 2\ CO_2 + 9\ H_2O + 2\ CH_4 + C_2H_6 + C_3H_8 + C_4H_{10} + H_2$	(1-S_O)–3.81	
		14 $CH_3OH \rightarrow$ Coke + 14 H_2O + 3 CH_4	3.81	
Regeneration reactor	Operating conditions	T [°C] / p [bar]	500 / 3	[53,61]
	Reaction parameter	Coke combustion [%]	100	[53,61]
Oligomerization	Operating conditions	T [°C] | p [bar]	250 | 50	[14,15,62]
	Reaction parameter according to Eq. (9)	x	RC: 3; PV: 2 | 3 | 4	–
		α	RC: 0.69; PV: 0.60–078[b]	–
	Inert gas fraction, controlled by recycle purge		30	–
Hydrogenation	Operating conditions	T [°C] | p [bar]	300 | 50	[44,46,62]
	Reaction parameter	Conversion [%]	100	[44,63]

[a] %$_C$: percentage of carbon input, [b] see supplementary information, section 2.2.

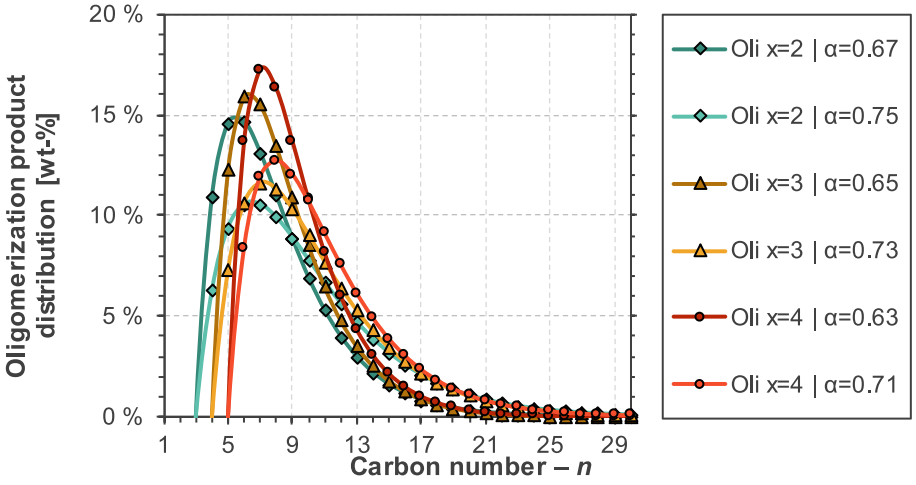

Fig. 9. Exemplary oligomerization product distributions according to model assumptions (α: Chain growth probability; Oli: Oligomerization; x: Parameter of Eq. (9)).

of mainly C_2 to C_4, besides the chain growth probability (α), starting point variation of ASF distribution is also considered through a parameter variation (section 4.2). This is conducted via an additional parameter referred to as x in this analysis (Eq. (9)). Some of the adjusted ASF distributions are exemplarily shown in Fig. 9. Hydrogenation is modeled analogously to FT syncrude upgrading.

An ASF distribution starting at butene ($x = 2$) could be representative for an ethene-based oligomerization with complete conversion. An x-value of 3 leads to a starting point at pentene, which can correspond to an ethene-propene dimer. A completely propene-based oligomerization could lead to a starting point at hexene – assuming complete conversion. Nevertheless, since oligomerization from an olefin mixture is generally assumed, both even and odd carbon chains are present in the product.

4. Results and discussion

In this section, the results of the flowsheet simulation are presented and assessed. First, the simulation results are shown in terms of carbon and energy flows. Additionally, the hydrogen flows are depicted in the supplementary information, section 3. The influences of the varied technical parameters on carbon and energy efficiency are presented in the process assessment. Subsequently, the process-specific results of the FT and methanol pathways are comparatively discussed and shown as PtL efficiency (incl. H_2 and CO_2 supply).

4.1. Process simulation

The process simulation results are used to visualize and evaluate the relative carbon and energy flows of the reference case processes.

4.1.1. Carbon flows

Below, the carbon flows are expressed in relation to the overall carbon input stream for both processes. Theoretically, the carbon can be entirely bound in the kerosene since no carbon-containing by-products occur within the main building reactions. However, due to impurities, side reactions, and only limited controllable chain length distributions, by-products, and carbon losses occur, which are visualized in the flow diagrams (Fig. 10 and Fig. 11).

4.1.1.1. Fischer-Tropsch pathway. Fig. 10 shows the relative carbon flows of the analyzed FT plant concept. The only carbon input into the process is the CO_2 input stream. This CO_2 is supplied to the RWGS reactor along with the synthesis gas recycle (in terms of carbon,

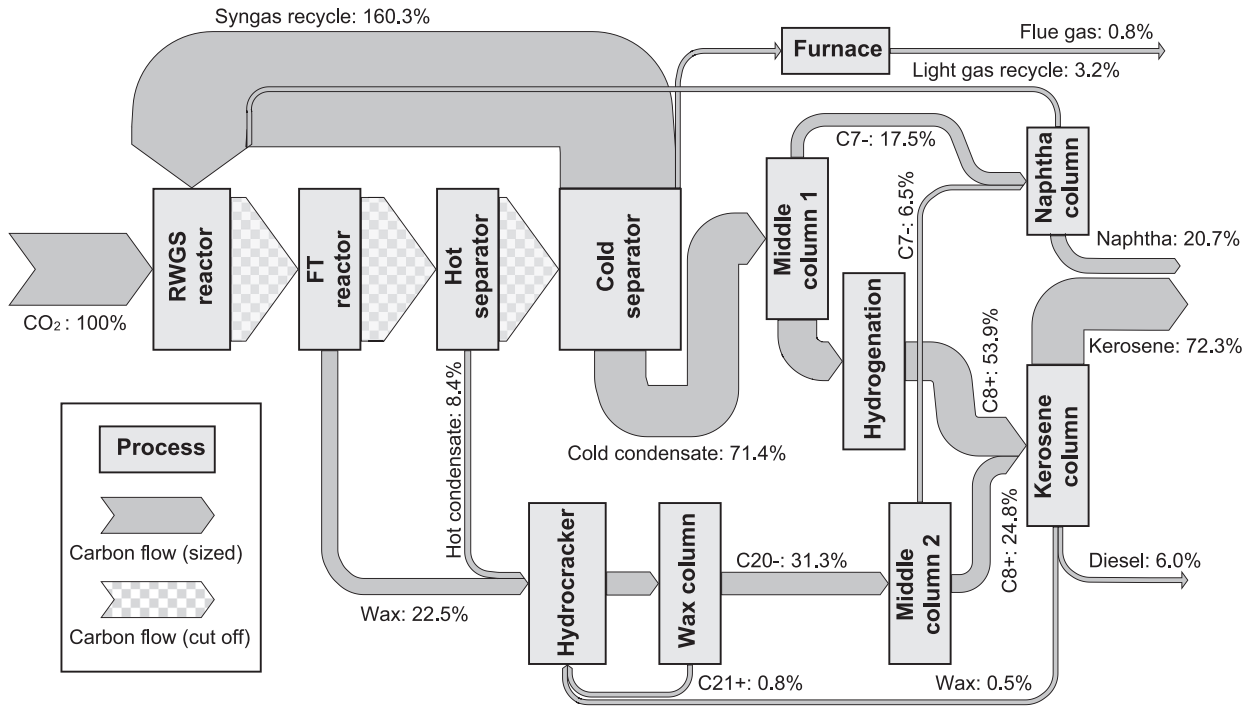

Fig. 10. Relative carbon flows of the FT pathway (only carbon flow affecting process blocks are shown; RWGS: Reverse water–gas shift).

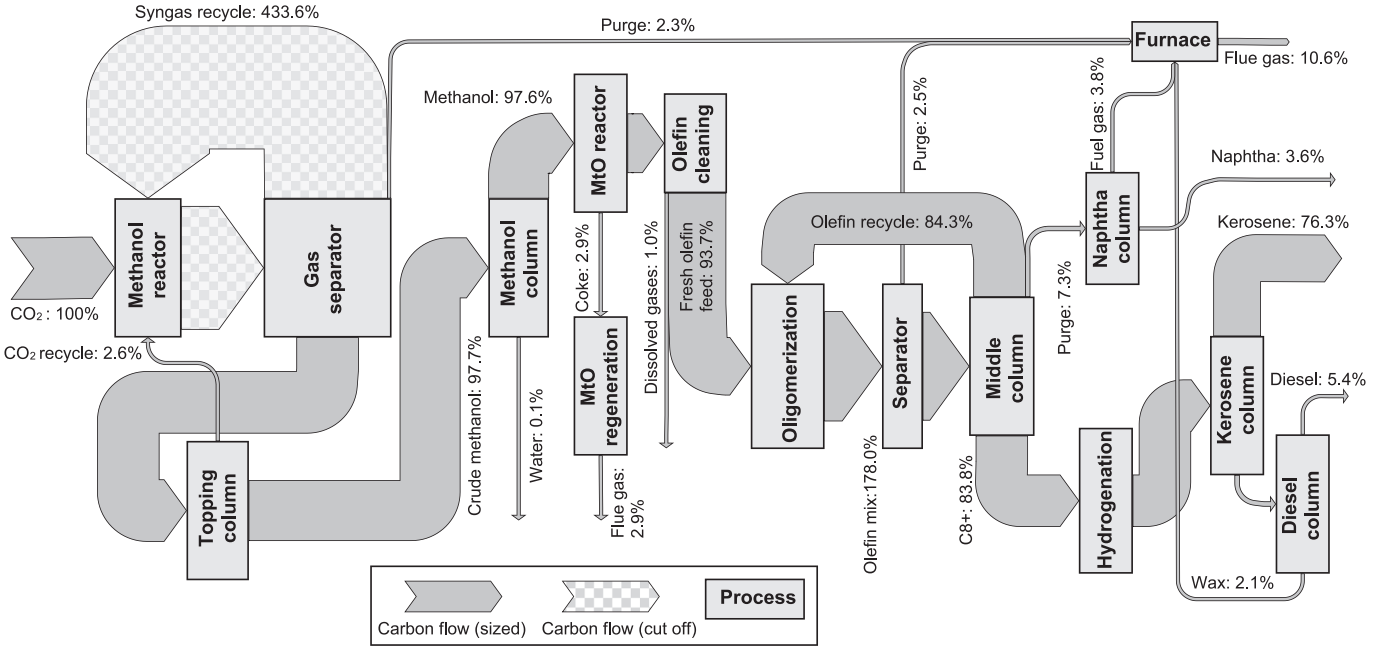

Fig. 11. Relative carbon flows of the methanol pathway (only carbon flow affecting process blocks are shown; MtO: Methanol-to-Olefins).

primarily CO, CO_2, and CH_4). Despite the high operation pressure, the high temperature suppresses methane formation within the RWGS reactor. As the methane formed in the FT reactor is largely recycled, RWGS methane reforming outweighs methane formation (RWGS feed: 5.1 mol%$_{CH4}$, RWGS product: 4.4 mol%). To prevent the accumulation of inert components, a purge gas stream is diverted from the recycle stream (cold separator) and exits the process after combustion in the form of CO_2 in the flue gas; this results in carbon losses of less than 1 %. Other carbon losses, such as dissolved components in wastewater, are below 0.1 % (and thus not shown in Fig. 10).

Downstream, approximately 30 % of the FT product consists of heavy components (wax and hot condensate) directed to the hydrocracking unit. Around 7 % of the hydrocracking products are light components (C_{7-}), while about 25 % are within the kerosene and diesel fraction (C_{8+}). The cold condensate divides into about 18 % naphtha and lighter components (C_{7-}) and approx. 54 % kerosene and heavier components (C_{8+}). The light and heavy fractions are fed to a naphtha column and a kerosene column, respectively, to obtain the individual target product fractions. Here, 73 % of the produced liquid products account for the target product kerosene, 21 % for naphtha, and only 6 % for diesel.

4.1.1.2. Methanol pathway. The relative carbon flows of the methanol pathway are shown in Fig. 11. Again, the CO_2 stream serves as the only carbon input. Upstream, methanol production yields a carbon efficiency of almost 98 %, with purge gases being the only significant losses. The major carbon losses occur downstream (i.e., in the MtK process section). During methanol dehydration, approximately 3 % of the carbon is discharged from the process as coke, which is released as CO_2 in the subsequent catalyst regeneration. In the oligomerization process, carbon losses occur due to removing light alkanes (purge from separator) and regulating inert components (middle column purge), amounting to about 3 and 7 %. The latter can be added to the naphtha fraction in certain proportions. Additionally, carbon losses occur due to heavy components (wax) utilized as an energy carrier within the furnace.

With regard to the carbon flows, the kerosene fraction accounts for almost 90 % of the liquid products, while naphtha and diesel represent only 4 % and 6 %, respectively.

4.1.2. Energetic flows

The specific energy flows are normalized to the total energy input of each pathway to analyze and assess the major energy demands and losses of the process concepts. Thereby, chemical energy (related to the higher heating value), electrical power, as well as heating and cooling demands (thermal energy) are distinguished as energy streams.

4.1.2.1. Fischer-Tropsch pathway. In the FT pathway (Fig. 12), hydrogen input accounts for 89 % of the total energy input. The FT synthesis operates at a relatively low pressure level (25 bar) (i.e., no further hydrogen compression is needed). Additionally, the comparatively high syngas conversion of 65 % leads to a rather low recycling ratio. This results in an electricity demand for compression below 2 % of the total energetic input. However, there is a high energy demand for the RWGS process, which cannot be fully supplied through heat integration alone and requires significant additional thermal energy provided by electricity (electrical heating). Due to the efficient recycling steps upstream and further downstream processing of by-products, only a small amount of heat is generated from combusting waste streams in the furnace. A significant cooling demand arises from the FT synthesis and the product condensation. After heat integration, the overall cooling demand via cooling water is estimated at 9 %, while a further 24 % of the energy can be used for external steam supply; i.e., about 33 % of the energy used in the process is dissipated in the form of heat. Around 10 % of the overall energy is required for heating demands and is provided by electricity. At the end of the overall process, 67 % of the input energy exits in the form of liquid products. Of this, 73 % can be allocated to the kerosene fraction, resulting in a kerosene energetic efficiency of 49 %.

4.1.2.2. Methanol pathway. In the methanol pathway (Fig. 13), the hydrogen input accounts for 94 % of the total energy input. Around 6 %

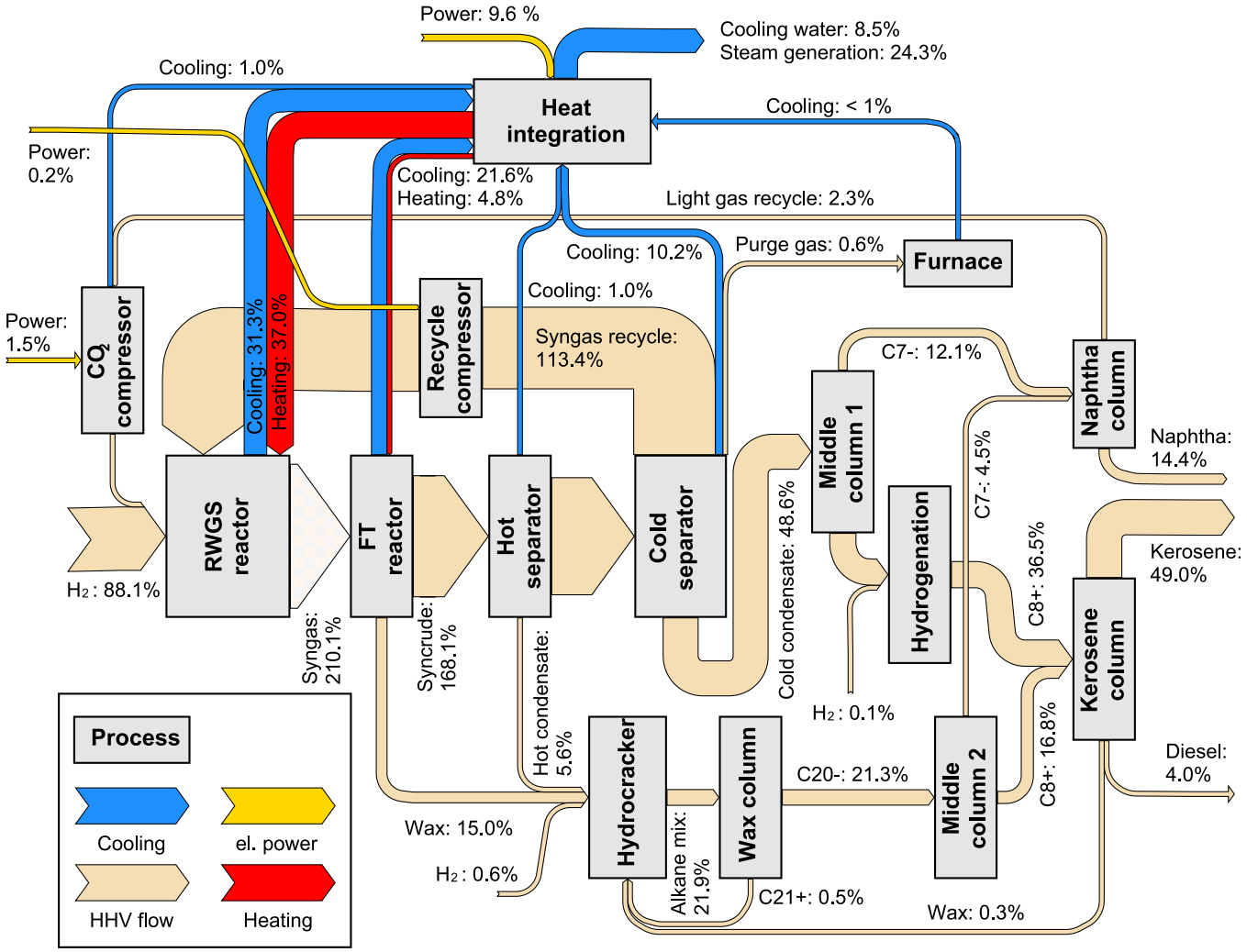

Fig. 12. Relative energy flows of the FT pathway (heating and cooling below 1% not depicted; HHV: Higher heating value; RWGS: Reverse water–gas shift).

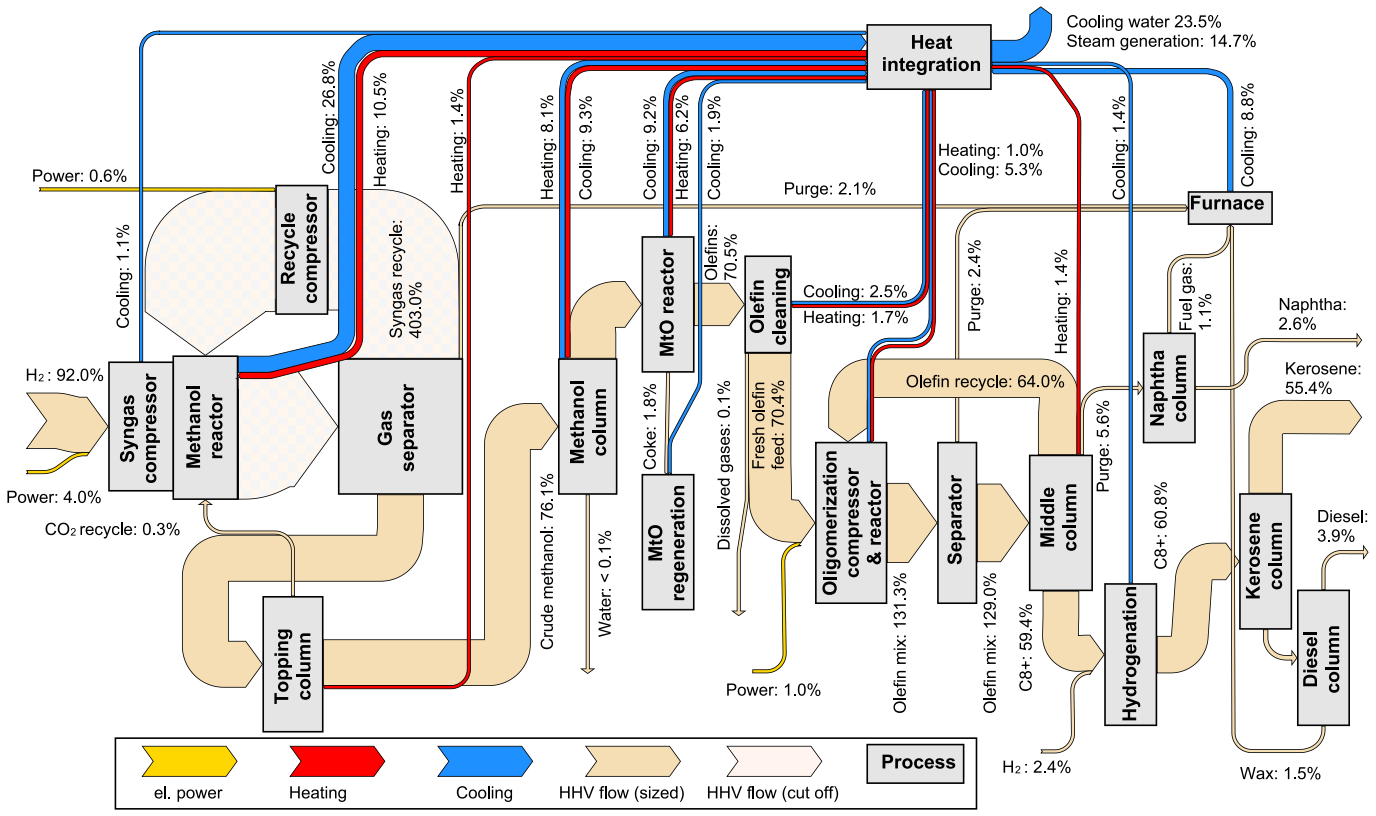

Fig. 13. Relative energy flows of the methanol pathway (heating and cooling below 1% not depicted; MtO: Methanol-to-Olefins).

of the total energy input (electrical power) is consumed for gas compression, particularly for the high pressures required for methanol synthesis. As all conversion processes are exothermic, no externally provided heat is required. There are losses associated with the exothermic methanol synthesis reaction. However, significant amounts of heat are needed for methanol purification. The combustion of waste streams generates heat at higher temperature levels (>900 °C) but leads to lower energy efficiency for the production of liquid fuel products at the same time. After heat integration, the overall cooling demand is estimated to be 38 % (i.e., 62 % cooling water and 38 % steam generation). The liquid product of the process accounts for 62 % of the total energy input; the kerosene fraction amounts to 90 % of these.

4.2. Process assessment

Based on the simulation results described above, the process assessment is carried out. The carbon efficiencies (section 4.2.1) and energy efficiencies (section 4.2.2) of the overall pathways are derived for the reference cases, while the influences of the underlying technology parameter assumptions are assessed through parameter variation. The sensitivity of the key figures regarding the varied parameters also indicates uncertainties and potentially desirable parameter ranges for optimized production.

4.2.1. Carbon efficiency

The relative carbon flows shown in section 4.1.1 represent the carbon efficiencies (section 2.3) of the individual product fraction. Fig. 14 presents the carbon efficiencies applied over the chain growth probability resulting from the simulation of the overall plant. Minor changes compared to the reference case (<1%) result from simplified rectification models in parameter variation simulation (supplementary information, section 2). Below, the results of the FT and the methanol pathway are described.

4.2.1.1. Fischer Tropsch pathway. In the reference case (secondary hydrocracking, $\alpha = 0.85$), the kerosene (K) carbon efficiency, which refers to the kerosene fraction, is around 72 %. Together with the naphtha and diesel fractions, this results in an almost ideal total product (TP) carbon efficiency of 99 %. In Fig. 14, left, the influences of the assumed chain growth probability and the considered hydrocracking behaviors on the carbon efficiency are depicted.

- Influence of chain growth probability (α). The chain growth probability is uniformly varied around the reference case ($\alpha = 0.85$), representing the maximum for straight-run kerosene. The TP carbon efficiency shows minimal changes over the variation range (98 to 99 %). The trend gradually increases, reaching a maximum of 99 % at α-values of 0.90. Shifting left from the maximum, lighter components in the syncrude increase, requiring reforming through the RWGS process and recycling into the synthesis loop. As recycling increases, losses through purge gases increase, leading to decreased TP efficiency. Higher α-values also increase the wax content that subsequently undergoes hydrocracking. The resulting light by-products are also fed back into the RWGS and subsequently into the synthesis loop. As cracking intensifies, the quantity of lighter components formed in the hydrocracker outweighs those formed in the synthesis, leading to a decline in TP efficiency to the right of the maximum with further increasing chain growth probabilities. Regarding the carbon efficiency of K, the maximum shifts towards higher α-values. This is because the decrease in straight-run kerosene is less significant up to a certain point compared to the increase in kerosene formed through hydrocracking. After this chain growth probability is reached, the K carbon efficiency decreases as the diesel fraction within the cracking products increases. This decrease is particularly evident in the case of primary and secondary cracking, as significantly more C_{17}-C_{20} molecules are formed here, which are subsequently not recycled in the wax column but are removed as diesel in the kerosene column.

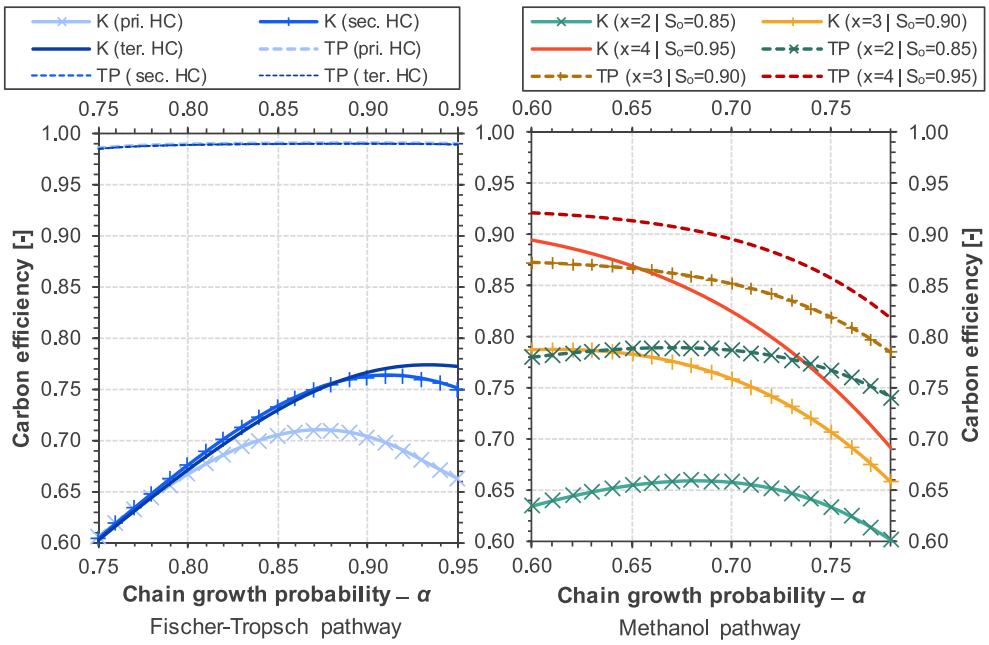

Fig. 14. Carbon efficiencies of overall Fischer-Tropsch and methanol pathway under parameter variation (HC: Hydrocracking, K: Kerosene, pri.: Primary, sec.: Secondary, S_O: Olefin-selectivity, ter.: Tertiary, TP: Total product, x: Parameter of Eq. (9)).

Therefore, the location of the maximum kerosene efficiency depends on the hydrocracking behavior considered.

- Influence of hydrocracking behavior. The variation of the hydrocracking behavior comprises three cases in which the number of cracking events per pass is varied (section 3.2.1). Across all three cracking cases, the K carbon efficiency values range from 60 to 77 %, depending on the α-value. In the case of primary cracking, for chain growth probabilities higher than 0.80, the K carbon efficiency is clearly lower than in the other hydrocracking cases, and thus also the maximum K carbon efficiency (71 % at $\alpha = 0.87$). However, this maximum shifts towards α-values above 0.90 for secondary and tertiary hydrocracking, with over 76 % ($\alpha = 0.91$, secondary cracking) and 77 % ($\alpha = 0.94$, tertiary cracking) of the carbon input bound in kerosene. The differences in K carbon efficiencies concerning the considered cracking scenarios primarily arise from the differential cracking of the diesel fraction (C_{17} to C_{20}). While, in the case of primary cracking, the diesel fraction is separated from the product mixture after hydrocracking, substantial portions of the fraction undergo further cracking in secondary and tertiary processes, diverting them to the naphtha and kerosene fractions instead of ending up in the diesel fraction. Even if the number of cracking operations cannot be controlled to the same extent as in the simulation, the same effect can be achieved in actual plant operation by selectively feeding diesel components back into the hydrocracker, which also allows higher kerosene efficiencies.

4.2.1.2. Methanol pathway. In the reference case of the methanol pathway ($S_O = 90$ %, $x = 3$, $\alpha = 0.69$), a TP carbon efficiency of about 85 % is obtained, while the K carbon efficiency reaches 76 %. Fig. 14, right, illustrates the influences of the ASF starting point (parameter x of Eq. (9)) and the considered olefin-selectivity over the chain growth probability (α). To independently assess the individual impacts of the varied parameters, the carbon efficiency profiles for the assumed olefin-selectivities are presented separately in Fig. 15. Subsequently, the influences of the varied parameters are explained separately. However, the influences of the varied parameters are partially interdependent. As a result, the effects cannot be discussed completely separately from each other.

- Influence of chain growth probability (α). The chain growth probability is varied below the α-value of maximum straight-run kerosene output (supplementary information, section 2.2). This is done because, in the overall process, the lighter naphtha fraction is fed back into the oligomerization, potentially increasing the overall kerosene fraction. The results of the parameter variation confirm this effect since a lower α-value generally leads to a higher K carbon efficiency. Furthermore, the TP efficiency is also positively influenced in most cases by a lower α-value, as the wax fractions (used only energetically) decreases.
- Influence of olefin-selectivity (S_O). The results of the parameter variation show that the olefin-selectivity is a decisive parameter which strongly affects the achievable carbon efficiencies. At an olefin-selectivity of 85 % the K carbon efficiency and the TP carbon efficiency are limited to 60 to 73 % and 74 to 82 %, respectively. Raising the olefin-selectivity to 95 %, K carbon efficiency and the TP carbon efficiency are increased to 69 to 90 % and 82 to 92 %, respectively. Direct losses caused by non-ideal olefin-selectivity occur as by-products (alkanes) do not oligomerize and are therefore not further processed into any of the desired product fractions. Indirect losses additionally arise due to the increasing purge requirements with rising amounts of inert alkanes, as this also results in the removal of more valuable olefins – i.e., olefins that could be further processed into the desired product fractions.
- Influence of ASF starting point. The impact of the ASF starting point – which approximates the influence of the olefin-feedstock (monomer) size – on the overall process is also dependent on S_O, which is evidently illustrated by different diagrams. At rather low olefin-selectivities ($S_O = 0.85$), a positive influence of larger monomers as oligomerization feed (higher x-values) can be observed. However, this influence of the monomer size on both the K and the TP carbon efficiency decreases significantly with increasing olefin-selectivities. At higher S_O-values, the carbon efficiencies achieved become increasingly less dependent on the monomer size. Additionally, with higher chain growth probabilities and particularly at increasing S_O-values, the influence of the monomer size even reverses; i.e., the achievable carbon efficiencies decrease as the monomer size increases. This inverse effect is observed for olefin-selectivities of $S_O = 0.95$ when the chain growth probabilities exceed approximately 0.65

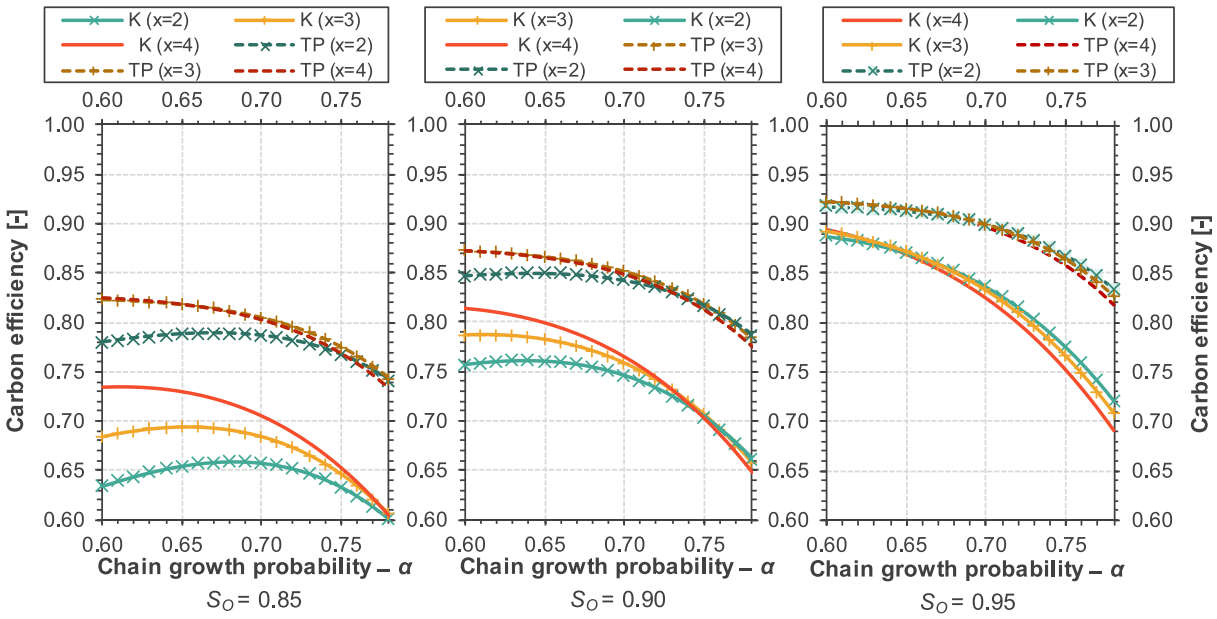

Fig. 15. Carbon efficiencies of overall methanol pathway under separate S_O and x-variation. (K: Kerosene, S_O: Olefin-selectivity, TP: Total product, x: Parameter of Eq. (9)).

for K carbon efficiency and 0.68 for TP carbon efficiency. The decreasing impact of ASF starting point with increasing S_O primarily results from a lower purge requirement, allowing for more efficient recycling of lighter naphtha. The transition from a positive to a negative effect of larger monomer sizes with increasing chain growth probabilities regarding the K carbon efficiency is primarily due to the shift of the straight-run kerosene fraction towards diesel. Regarding the TP carbon efficiency, this effect is primarily attributed to increased wax formation with higher chain growth probabilities.

Across all variations, the methanol pathway shows high kerosene yields, especially for chain growth probabilities well below the straight-run optimum. This is primarily a result of the direct recycling of the light naphtha fraction. The olefin-selectivity (S_O) of the MtO process is identified as a crucial process parameter, as it strongly influences both kerosene yield and overall yield under the assumptions made. The results suggest that a high olefin-selectivity is more important for the efficiencies of the process than a high straight-run kerosene fraction. Furthermore, the results obtained by the underlying assumptions suggest that low chain growth probabilities starting from higher olefins ($x = 4$) achieve higher kerosene yields than starting from very light olefins ($x = 2$) with higher chain growth probabilities. Starting from higher olefins might also influence the smoothness of the product distribution, which is not analyzed here.

4.2.2. Energy efficiency

Fig. 16 shows the energy efficiencies applied over the chain growth probability (α) resulting from the simulation of the overall plant. Minor changes compared to the base case analysis (<1 %) result from simplified fractionation models in parameter variation (see supplementary information, section 2). Based on the higher heating values (HHV), a theoretical maximum energy efficiency of 77 % can be cited. This theoretical efficiency is calculated by dividing the energy of the products (assumed here to be $C_{10}H_{22}$ and H_2O) by that of the reactants (H_2 and CO_2), and thus takes into account the losses of the reaction enthalpy of the overall reaction. Since the energy streams of the product fractions are proportional to the respective carbon flows, carbon efficiency directly affects energy efficiency. Furthermore, the main energy input of both pathways results from hydrogen, which also supports a correlation of energy with carbon efficiency as a parameter of material utilization. In tendency, the effects are, therefore, similar to the results shown in Fig. 14. However, the variation of technical parameters influences internal process flows and energy requirements, eventually affecting energy efficiency. The resulting deviations from the carbon efficiency and the key figure areas are explained below.

4.2.2.1. Fischer-Tropsch pathway. The energy efficiency in the reference case shown in section 4.1.2 is determined to be 49 % with regard to the energy content of the produced kerosene. The TP energy efficiency, considering the naphtha, kerosene, and diesel fraction, reaches 67 %. Fig. 16 left, shows the influence of the assumed chain growth probability and the considered hydrocracking behavior on the energy efficiency.

- Influence of chain growth probability (α). The TP energy efficiency shows a stronger sensitivity regarding the chain length probability compared to the carbon efficiency, ranging from 63 to 70 %. This is because at low α-values, the amount of light components reformed in the RWGS (reverse water–gas shift) process significantly increases. The additional energy required for this needs to be covered by external energy (electrical power), resulting in an overall increase in energy demand while the fuel product quantity remains nearly constant. Regarding kerosene, the amount of produced kerosene (carbon efficiency) increases and the required energy quantity in the RWGS process decrease with increasing α-values. Therefore, the K energy efficiency still varies in a larger range from 39 to 54 %. The changes in compressor power due to varying process streams are negligible with respect to the overall energy demand.
- Influence of hydrocracking behavior. Between the hydrocracking cases, energy efficiencies behave almost identically to the carbon efficiencies. This is because the different hydrocracking cases have no significant impact on the energy requirements of the overall process, which means that energy efficiency correlates directly with the product quantity.

4.2.2.2. Methanol pathway. The K energy efficiency of the methanol pathways reference case is determined to be 55 %, while the TP energy efficiency amounts to about 62 %. Fig. 16 right, shows the influence of the considered ASF starting points and olefin-selectivity over the chain growth probability on the energy efficiency. The results of the parameter variation show a wide range of K energy efficiency (44 to 65 %) and the

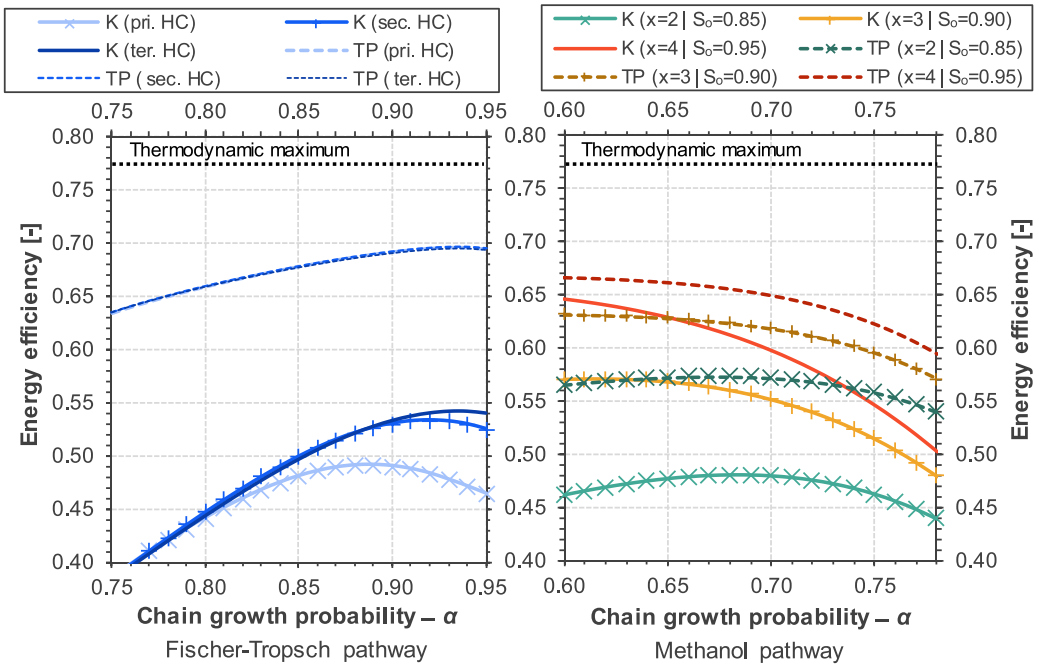

Fig. 16. Energy efficiencies of overall Fischer-Tropsch and methanol pathway under parameter variation (HC: Hydrocracking, K: Kerosene, pri.: Primary, sec.: Secondary, S_O: Olefin-selectivity, ter.: Tertiary, TP: Total product, x: Parameter of Eq. (9)).

TP energy efficiency (54 to 67 %).

Since the energy efficiency in the methanol pathway is almost exclusively influenced by the material efficiency, the resulting curves from parameter variation behave similarly to those of the carbon efficiency. More precisely, this is because the varied parameters have no influence on the methanol production efficiency, and changes in the oligomerization recycle with regard to the compressor power are below 0.5 %. For the discussion of the individual influences of the varied parameters, reference is made to the above-described section on carbon efficiency.

4.2.2.3. Overall comparison. The key figures of both pathways are compared in Fig. 17. In the following, these are discussed for the carbon efficiency and the energy efficiency. To enable an assessment of the pathways in relation to the entire PtL process chain, the provision of the feedstocks H_2 and CO_2 is additionally included in the energy efficiency at the end of this section.

4.2.3. Carbon efficiency

4.2.3.1. Total product carbon efficiency. Compared to the methanol pathway, the FT pathway enables a higher TP carbon efficiency through upstream reforming of lighter components and downstream hydrocracking of heavier components, with only minor losses occurring in the synthesis loop. The carbon efficiency sums up to approximately 99 %, varying only within a relatively small range within the parameter variation. While the methanol synthesis itself is highly selective, the lower per-pass conversion results in purge losses exceeding those of the FT synthesis. However, the major carbon losses in the methanol pathway occur in the MtK process due to a limited selectivity in dehydration,

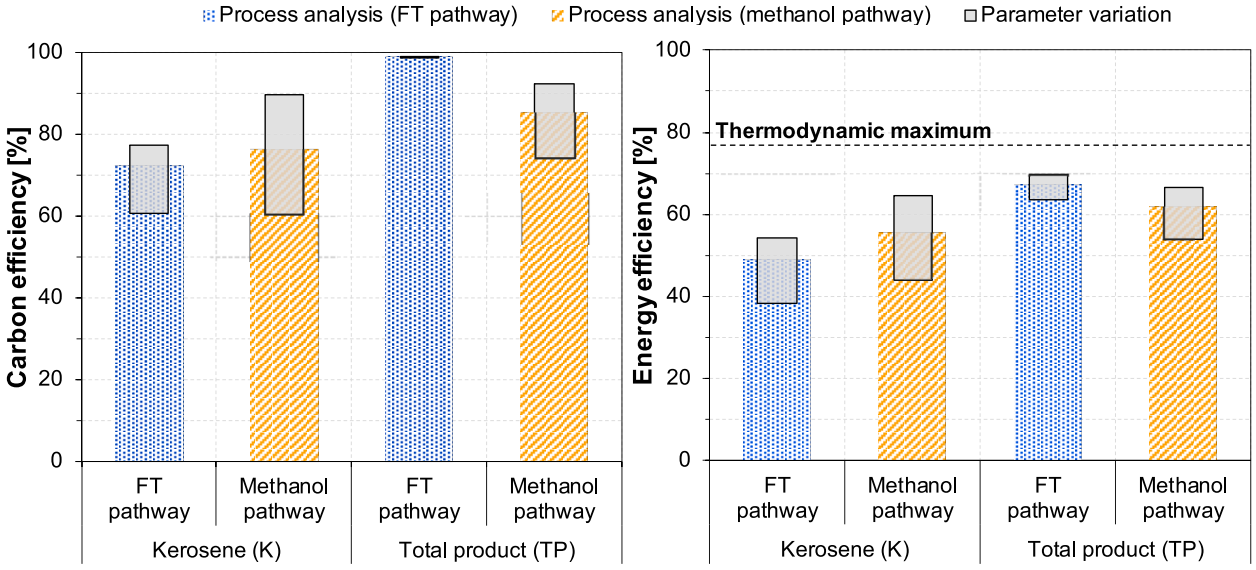

Fig. 17. Key overall figures of the FT and methanol pathway (FT: Fischer-Tropsch).

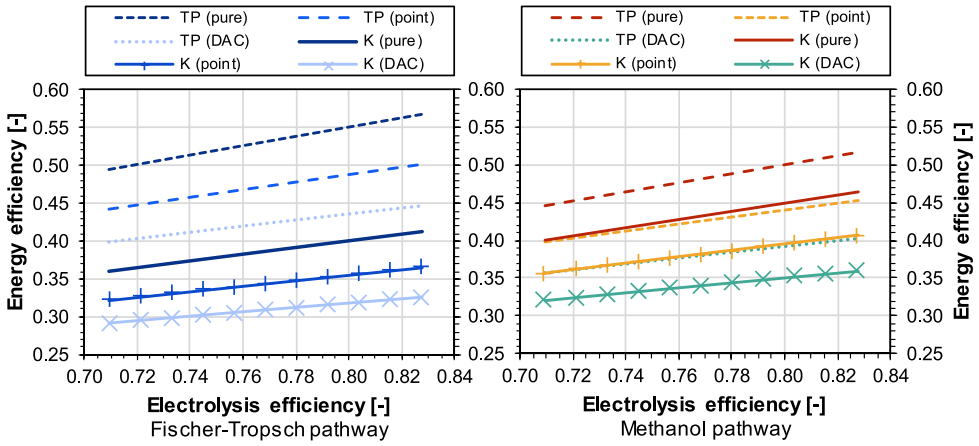

Fig. 18. Energy efficiency considering H_2 production and CO_2 supply (All efficiencies based on HHV; DAC: Direct air capture, K: Kerosene, point: CO_2 point source, pure: Pure CO_2, TP: Total product).

which also determines carbon losses in oligomerization. Overall, this leads to a lower TP carbon efficiency of about 85 %. The value shows a higher variation from 74 to 92 % in the parameter variation compared to almost constant TP carbon efficiency in the FT pathway.

4.2.3.2. Kerosene carbon efficiency. Despite the overall carbon losses, in the reference case the methanol pathway has a higher K carbon efficiency (76 %) compared to the FT pathway (72 %). This is due to the narrower product distribution and the recycling of the light naphtha product fraction. Nevertheless, depending on the parameters considered, the parameter variation shows a wide range from 60 to 90 %, whereby the influence on the technical parameters and, thus, the achievable efficiencies currently appear to be limited. The range in the FT pathway is also comparably wide, reaching from 61 to 77 %. However, since the chain growth probability in the FT synthesis can be well adjusted through catalysts and process conditions, optimizing the overall process towards the upper values of kerosene efficiency is realistic.

In addition to the kerosene yield, the composition of the fraction also differs (supplementary information, section 3.2). The methanol pathway analyzed here yields a kerosene fraction with a high proportion of light components. In contrast, the kerosene fraction formed in the FT pathway is more uniform and potentially easier to process into ASTM-compliant fuel.

4.2.4. Energy efficiency

The comparison of the FT against the methanol pathway depicted in Fig. 17, shows that, compared to the carbon efficiency (left), the methanol pathway has shifted upwards in terms of the energy efficiency (right). This can be explained due to the thermodynamic advantage of the methanol pathway, where only exothermic processes occur, and no additional energy is required for CO_2 reduction or recycle gas reforming.

4.2.4.1. Total product energy efficiency. Concerning energy efficiency, hydrogen is the largest energy input for both pathways. The FT pathway also requires a significant additional heating demand, mainly caused by the RWGS. In the methanol pathway, all reaction steps are exothermic, allowing to cover all heating demands through heat integration. However, higher electrical energy requirements for compression are needed compared to the FT pathway. Due to the low material losses, manifesting as energy losses due to combustion in the furnace, the FT pathway achieves higher total product (TP) energy efficiencies (67 %) than the methanol pathway (62 %) in the reference case. The parameter variation of the FT pathway shows a wider range of TP energy efficiency (63 to 70 %) compared to the TP carbon efficiency. This is due to an increasing energy demand of the RWGS at lower chain growth probabilities, which leads to a higher reforming effort. In contrast, almost no energetic influences besides the material efficiency occur in the methanol pathway; i.e., the energy efficiency behaves similarly to its carbon efficiency ranging from 54 to 67 %.

4.2.4.2. Kerosene energy efficiency. In terms of K energy efficiency, both pathways show a similar behavior as with regard to carbon efficiency. However, the methanol pathway is more clearly above the FT pathway in terms of energy than is the case for carbon. The reference case results are 55 % and 49 %, respectively. The methanol pathway ranges from 44 to 65 %, while the FT pathway reaches 38 to 54 %. Comparing the lower end of the K efficiencies demonstrates the thermodynamic advantage of the methanol pathway. While both pathways are almost equal in terms of carbon, the methanol pathway exceeds the FT pathway in terms of energy by more than 5 %pt..

4.2.4.3. Power-to-Liquid efficiency. The previously discussed efficiencies pertain to the system boundaries chosen within the analysis, i.e., H_2 and CO_2 are available as pure components. To make statements about the efficiencies of the entire production chain of electricity-based kerosene, the efforts or losses in feedstock supply must be considered. The energy efficiency starting from electrical power, including H_2 provision and CO_2 capture, is depicted in Fig. 18. The energy requirements of electrolysis depend on the chosen technology and vary within the efficiency range for low-temperature electrolyzers. The energy expenditure for CO_2 capture is highly contingent on the CO_2 source and the availability of heat ($T > 100$ °C). The illustration distinguishes three cases. In one case, pure CO_2 ("pure"), e.g., from ethanol fermentation, is considered, eliminating the need for further efforts. Case two ("point") represents capture via amine scrubbing from point sources (10–40 vol-% CO_2). Additionally, capture through a direct air capture facility ("DAC") is considered. In both capture cases, no heat integration is assumed.

Depending on the electrolyzer efficiency, the total product (TP) efficiency in both pathways decreases by 10–18 %pt.. The overall efficiency is thus 49–57 % (46–53 $\%_{LHV}$) for the FT pathway and 45–52 % (41–48 $\%_{LHV}$) for the methanol pathway. If CO_2 needs to be additionally captured from a point source with no heat integration possible, the efficiency further decreases by approximately 6 %pt. to 44–50 % (41–47 $\%_{LHV}$) for the FT pathway and 40–45 % (37–42 $\%_{LHV}$) for the methanol pathway. In the absence of a point source, requiring CO_2 to be captured from the air, the efficiencies further decline to 40–45 % (37–42 $\%_{LHV}$) for the FT pathway and 36–40 % (33–37 $\%_{LHV}$) for the methanol pathway. The provision of feedstocks H_2 and CO_2 plays a significant role in overall efficiency. Since the efficiency of synthesis and downstream processes directly determines the demand for feedstock, any conversion losses occurring here directly increase the losses in feedstock provision.

5. Conclusion

This research paper investigates and compares the FT and methanol pathway from power-derived syngas within an in-depth technical analysis. The main findings can be summarized as follows.

- Concerning carbon efficiency, the FT pathway enables very high efficiencies regarding to the total product (TP) yield (approx. 98 to 99 %). However, due to FT synthesis's relatively broad product distribution, the specific kerosene selectivity and, thus, the kerosene (K) carbon efficiency are clearly lower (approx. 61 to 77 %). The concept of the methanol pathway exhibits a higher K efficiency (approx. 60 to 90 %) but a significantly lower TP efficiency (approx. 74 to 92 %). This is due to, on the one hand, the high proportion of straight-run kerosene and the recycling of light olefins (naphtha fraction), but, on the other hand, losses through limited olefin-selectivities and the inability to further process heavy components.
- Concerning energy efficiency, hydrogen feed accounts for the highest energy input in both pathways, constituting more than 89 %. Therefore, energy efficiency is closely linked to material efficiency, meaning that higher material or hydrogen losses within the overall process result in a lower energy efficiency. Consequently, due to minor material losses, the FT pathway shows a higher TP energy efficiency of 67 % (72 $\%_{LHV}$) compared to the methanol pathway with 62 % (67 $\%_{LHV}$). However, the latter still shows a higher kerosene energy efficiency of 55 % (60 $\%_{LHV}$) against 49 % (53 $\%_{LHV}$) within the FT pathway. Also, the methanol pathway offers advantages since no high-temperature heat is required. In the FT pathway, the RWGS synthesis necessitates significant energy input, which is subsequently released at a lower energy level in the FT synthesis. A CO_2-based methanol synthesis ensures that the entire methanol pathway consists of exothermic processes and minimizes losses from a thermodynamic perspective. To determine the overall PtL efficiency, the H_2 and CO_2 supply must also be taken into account, which significantly reduces the energy efficiencies of the overall production.
- Based on the parameter variation, significantly higher uncertainties arise with regard to the evaluation of the methanol pathway. This is indicated by the strong sensitivity in K and TP efficiency, especially concerning the olefin-selectivity and the chain growth probability. In contrast, the FT pathway's assumptions, parameters, and results suggest lower uncertainties since more data are available in the literature, and the overall process shows lower sensitivities regarding the varied parameters.

Building upon this technical analysis, further theoretical considerations can be pursued to enable a more comprehensive evaluation of the two pathways. This includes additional technical analysis considering different plant concepts (e.g., 100 % kerosene plants or combined technology approaches) and economic and environmental analysis. Furthermore, theoretical and practical product quality investigations are necessary to optimize both pathways in terms of yield and fuel quality.

Funding

This research did not receive any specific grant from funding agencies in the public, commercial, or not-for-profit sectors.

CRediT authorship contribution statement

Stefan Bube: Writing – review & editing, Writing – original draft, Visualization, Methodology, Investigation, Formal analysis, Data curation, Conceptualization. **Nils Bullerdiek:** Writing – review & editing, Conceptualization. **Steffen Voß:** Methodology, Validation. **Martin Kaltschmitt:** Supervision, Writing – review & editing.

Declaration of competing interest

The authors declare that they have no known competing financial interests or personal relationships that could have appeared to influence the work reported in this paper.

Data availability

Data will be made available on request.

Appendix A. Supplementary data

Supplementary data to this article can be found online at https://doi.org/10.1016/j.fuel.2024.131269.

References

[1] International Air Transport Association. Resolution on the industry's commitment to reach net zero carbon emissions by 2050: Press Release No: 66; 2021.
[2] International Civil Aviation Organization. Resolution A41-21.: Consolidated statement of continuing ICAO policies and practices related to environmental protection - Climate change. Montréal; 2022.
[3] Grewe V, Gangoli Rao A, Grönstedt T, Xisto C, Linke F, Melkert J, et al. Evaluating the climate impact of aviation emission scenarios towards the Paris agreement including COVID-19 effects. Nat Commun 2021;12(1):3841. https://doi.org/10.1038/s41467-021-24091-y.
[4] Kärcher B. Formation and radiative forcing of contrail cirrus. Nat Commun 2018;9(1):1824. https://doi.org/10.1038/s41467-018-04068-0.
[5] Lee DS, Fahey DW, Skowron A, Allen MR, Burkhardt U, Chen Q, et al. The contribution of global aviation to anthropogenic climate forcing for 2000 to 2018. Atmos Environ 1994;2021(244):117834. https://doi.org/10.1016/j.atmosenv.2020.117834.
[6] Bullerdiek N, Voß S, Neuling U, Kaltschmitt M. Direct alcohol vs. alcohol-to-jet SPK utilisation in commercial aviation – an energetic-operational analysis. Int J Sustainable Aviation 2022.
[7] Bullerdiek N, Quante G, Bube S, Neuling U, Kaltschmitt M. Non Drop-In Kraftstoffe im Luftverkehr – Ein gesamtsystemischer Vergleich von Nutzungs- und Einsatzmöglichkeiten. Berlin: Hamburg; 2022.
[8] Surgenor C. LanzaJet opens the world's first-of-a-kind ethanol to jet fuel production facility. [January 10, 2024]; Available from: https://www.greenairnews.com/?p=5251.
[9] Quante G, Bullerdiek N, Bube S, Neuling U, Kaltschmitt M. Renewable fuel options for aviation – a system-wide comparison of drop-in and non drop-in fuel options. Fuel 2023;333:126269. https://doi.org/10.1016/j.fuel.2022.126269.
[10] Schmidt P, Weindorf W, Roth A, Batteiger V, Riegel F. Power-to-Liquids: Potentials and Perspectives for the Future Supply of Renewable Aviation Fuel.
[11] de Klerk A. Fischer-Tropsch refining. Weinheim: Wiley-VCH; 2011.
[12] Dieterich V, Buttler A, Hanel A, Spliethoff H, Fendt S. Power-to-liquid via synthesis of methanol, DME or Fischer–Tropsch-fuels: a review. Energy Environ Sci 2020;13(10):3207–52. https://doi.org/10.1039/D0EE01187H.
[13] Panzone C, Philippe R, Chappaz A, Fongarland P, Bengaouer A. Power-to-liquid catalytic CO2 valorization into fuels and chemicals: focus on the Fischer-Tropsch route. J CO2 Util 2020;38:314–47. https://doi.org/10.1016/j.jcou.2020.02.009.
[14] Bertau M, Offermanns H, Plass L, Schmidt F, Wernicke H-J. Methanol: The Basic Chemical and Energy Feedstock of the Future. Berlin, Heidelberg: Springer, Berlin Heidelberg; 2014.
[15] Bellussi G, Mizia F, Calemma V, Pollesel P, Millini R. Oligomerization of olefins from Light Cracking Naphtha over zeolite-based catalyst for the production of high quality diesel fuel. Microporous Mesoporous Mater 2012;164:127–34. https://doi.org/10.1016/j.micromeso.2012.07.020.
[16] Kaltschmitt M, Neuling U (eds.). Biokerosene. Berlin, Heidelberg: Springer Berlin Heidelberg; 2018.
[17] Atsonios K, Li J, Inglezakis VJ. Process analysis and comparative assessment of advanced thermochemical pathways for e-kerosene production. Energy 2023;278:127868. https://doi.org/10.1016/j.energy.2023.127868.
[18] aspentech. Aspen Plus. Bedford: Aspen Technology Inc.
[19] Al-Malah KIM. Aspen plus: Chemical engineering applications. Hoboken, New Jersey: Wiley; 2017.
[20] Haydary J. Chemical process design and simulation: Aspen Plus and Aspen HYSYS applications. Hoboken, N.J.: Wiley; 2019.
[21] Schefflan R. Teach Yourself the Basics of Aspen Plus™. Wiley; 2011.
[22] Buttler A, Spliethoff H. Current status of water electrolysis for energy storage, grid balancing and sector coupling via power-to-gas and power-to-liquids: a review. Renew Sustain Energy Rev 2018;82:2440–54. https://doi.org/10.1016/j.rser.2017.09.003.
[23] Siemens Energy. Silyzer 300: The next paradigm of PEM electrolysis. [January 18, 2024]; Available from: https://assets.siemens-energy.com/siemens/assets/api/uuid:a193b68f-7ab4-4536-abe2-c23e01d0b526/datasheet-silyzer300.pdf.
[24] Fischedick M, Görner K, Thomeczek M. CO2: Abtrennung, Speicherung, Nutzung. Berlin, Heidelberg: Springer, Berlin Heidelberg; 2015.

[25] Pearson K. Hydrogen production by partial catalytic dehydrogenation of kerosene. Dissertation 2015.
[26] Schemme S. Techno-ökonomische bewertung von verfahren zur herstellung von kraftstoffen aus H2 und CO2. Energie & Umwelt / Energy Environ 2020.
[27] Kaltschmitt M, Hofbauer H, Lenz V. (ed.). Synthesen und Weiterverarbeitung: in Energie aus Biomasse. Band 2 - im Druck. Springer; 2023.
[28] Wei J, Ge Q, Yao R, Wen Z, Fang C, Guo L, et al. Directly converting CO2 into a gasoline fuel. Nat Commun 2017;8:15174. https://doi.org/10.1038/ncomms15174.
[29] Wang Y, Kazumi S, Gao W, Gao X, Li H, Guo X, et al. Direct conversion of CO2 to aromatics with high yield via a modified Fischer-Tropsch synthesis pathway. Appl Catal B 2020;269:118792. https://doi.org/10.1016/j.apcatb.2020.118792.
[30] Yang Q, Kondratenko VA, Petrov SA, Doronkin DE, Saraçi E, Lund H, et al. Identifying performance descriptors in CO2 hydrogenation over iron-based catalysts promoted with alkali metals. Angew Chem Int Ed Engl 2022;61(22):e202116517.
[31] Corrao E, Salomone F, Giglio E, Castellino M, Ronchetti SM, Armandi M, et al. CO2 conversion into hydrocarbons via modified Fischer-Tropsch synthesis by using bulk iron catalysts combined with zeolites. Chem Eng Res Des 2023;197:449–65. https://doi.org/10.1016/j.cherd.2023.07.052.
[32] Shi B, Davis BH. Fischer-Tropsch synthesis: the paraffin to olefin ratio as a function of carbon number. Catal Today 2005;106(1–4):129–31. https://doi.org/10.1016/j.cattod.2005.07.159.
[33] Kaiser P, Unde RB, Kern C, Jess A. Production of liquid hydrocarbons with CO 2 as carbon source based on reverse water-gas shift and fischer-tropsch synthesis. Chem Ing Tech 2013;85(4):489–99. https://doi.org/10.1002/cite.201200179.
[34] König DH. Techno-ökonomische Prozessbewertung der Herstellung synthetischen Flugturbinentreibstoffes aus CO2 und H2; 2016.
[35] Nestler F, Krüger M, Full J, Hadrich MJ, White RJ, Schaadt A. Methanol synthesis - industrial challenges within a changing raw material landscape. Chem Ing Tech 2018;90(10):1409–18. https://doi.org/10.1002/cite.201800026.
[36] Maus W. Zukünftige Kraftstoffe. Berlin, Heidelberg: Springer, Berlin Heidelberg; 2019.
[37] Sydora OL, Jones TC, Small BL, Nett AJ, Fischer AA, Carney MJ. Selective ethylene tri-/tetramerization catalysts. ACS Catal 2012;2(12):2452–5. https://doi.org/10.1021/cs300488t.
[38] Britovsek GJP, Malinowski R, McGuinness DS, Nobbs JD, Tomov AK, Wadsley AW, et al. Ethylene oligomerization beyond schulz-flory distributions. ACS Catal 2015;5(11):6922–5. https://doi.org/10.1021/acscatal.5b02203.
[39] Nicholas CP. Applications of light olefin oligomerization to the production of fuels and chemicals. Appl Catal A 2017;543:82–97. https://doi.org/10.1016/j.apcata.2017.06.011.
[40] Unde RB. Kinetics and reaction engineering aspects of syngas production by the heterogeneously catalysed reverse water gas shift reaction: Dissertation; 2012.
[41] Wolf A, Jess A, Kern C. Syngas production via reverse water-gas shift reaction over a Ni-Al 2 O 3 catalyst: catalyst stability, reaction kinetics, and modeling. Chem Eng Technol 2016;39(6):1040–8. https://doi.org/10.1002/ceat.201500548.
[42] Rezaei E, Dzuryk S. Techno-economic comparison of reverse water gas shift reaction to steam and dry methane reforming reactions for syngas production. Chem Eng Res Des 2019;144:354–69. https://doi.org/10.1016/j.cherd.2019.02.005.
[43] Rafati M, Wang L, Dayton DC, Schimmel K, Kabadi V, Shahbazi A. Techno-economic analysis of production of Fischer-Tropsch liquids via biomass gasification: the effects of Fischer-Tropsch catalysts and natural gas co-feeding. Energ Conver Manage 2017;133:153–66. https://doi.org/10.1016/j.enconman.2016.11.051.
[44] de Klerk A. Fischer-Tropsch refining: technology selection to match molecules. Green Chem 2008;10(12):1249. https://doi.org/10.1039/b813233j.
[45] Bouchy C, Hastoy G, Guillon E, Martens JA. Fischer-Tropsch waxes upgrading via hydrocracking and selective hydroisomerization. Oil & Gas Science and Technology - Rev IFP 2009;64(1):91–112. https://doi.org/10.2516/ogst/2008047.
[46] Lamprecht D. Hydrogenation of Fischer−Tropsch synthetic crude. Energy Fuels 2007;21(5):2509–13. https://doi.org/10.1021/ef060612q.
[47] Butera G, Fendt S, Jensen SH, Ahrenfeldt J, Clausen LR. Flexible methanol production units coupling solid oxide cells and thermochemical biomass conversion via different gasification technologies. Energy 2020;208:118432. https://doi.org/10.1016/j.energy.2020.118432.
[48] Haag S, Castillo-Welter F, Schuhmann T, Williams BA, Oelmann T, Günther A, et al. How to Convert CO2 to Green Methanol: Challenges for Petrochemicals and Fuels: Integration of Value Chains and Energy Transition. Berlin; 2018.
[49] Ott J, editor. Ullmann's Encyclopedia of Industrial Chemistry: Methanol. Weinheim, Germany: Wiley-VCH Verlag GmbH & Co. KGaA; 2012.
[50] Mbatha S, Everson RC, Musyoka NM, Langmi HW, Lanzini A, Brilman W. Power-to-methanol process: a review of electrolysis, methanol catalysts, kinetics, reactor designs and modelling, process integration, optimisation, and techno-economics. Sustain Energ Fuels 2021;5(14):3490–569. https://doi.org/10.1039/D1SE00635E.
[51] Gogate MR. Methanol-to-olefins process technology: current status and future prospects. Pet Sci Technol 2019;37(5):559–65. https://doi.org/10.1080/10916466.2018.1555589.
[52] Samanta C, Das RK. C3-Based Petrochemicals: Recent Advances in Processes and Catalysts. In: Pant KK, Gupta SK, Ahmad E, editors. Catalysis for Clean Energy and Environmental Sustainability. Cham: Springer International Publishing; 2021. p. 149–204.
[53] Ortiz-Espinoza AP, Noureldin MM, El-Halwagi MM, Jiménez-Gutiérrez A. Design, simulation and techno-economic analysis of two processes for the conversion of shale gas to ethylene. Comput Chem Eng 2017;107:237–46. https://doi.org/10.1016/j.compchemeng.2017.05.023.
[54] Independent Commodity Integrence Service. UOP/Hydro work MTO magic: MTO MATERIAL BALANCE. [October 18, 2021]; Available from: https://www.icis.com/explore/resources/news/1996/06/01/9793/uop-hydro-work-mto-magic/.
[55] Yang M, Fan D, Wei Y, Tian P, Liu Z. Recent progress in methanol-to-olefins (MTO) catalysts. Adv Mater 2019;31(50):e1902181.
[56] Ye M, Tian P, Liu Z. DMTO: a sustainable methanol-to-olefins technology. Engineering 2021;7(1):17–21. https://doi.org/10.1016/j.eng.2020.12.001.
[57] Kianfar E. Comparison and assessment of zeolite catalysts performance dimethyl ether and light olefins production through methanol: a review. Rev Inorg Chem 2019;39(3):157–77. https://doi.org/10.1515/revic-2019-0001.
[58] Vora BV, Marker TL, Barger PT, Nilsen HR, Kvisle S, Fuglerud T. Economic route for natural gas conversion to ethylene and propylene. In: Natural Gas Conversion IV. Elsevier; 1997. p. 87–98.
[59] Keil FJ. Methanol-to-hydrocarbons: process technology. Microporous Mesoporous Mater 1999;29(1–2):49–66. https://doi.org/10.1016/S1387-1811(98)00320-5.
[60] Dimian AC, Bildea CS. Energy efficient methanol-to-olefins process. Chem Eng Res Des 2018;131:41–54. https://doi.org/10.1016/j.cherd.2017.11.009.
[61] Avidan AA. Gasoline and distillate fuels from methanol. in: methane conversion, Proceedings of a Symposium on the Production of Fuels and Chemicals from Natural Gas. Elsevier; 1988, p. 307–323.
[62] Eagan NM, Kumbhalkar MD, Buchanan JS, Dumesic JA, Huber GW. Chemistries and processes for the conversion of ethanol into middle-distillate fuels. Nat Rev Chem 2019;3(4):223–49. https://doi.org/10.1038/s41570-019-0084-4.
[63] Tao L, Markham JN, Haq Z, Biddy MJ. Techno-economic analysis for upgrading the biomass-derived ethanol-to-jet blendstocks. Green Chem 2017;19(4):1082–101. https://doi.org/10.1039/C6GC02800D.